Pre–Steady-State Charge Translocation in NaK-ATPase from Eel Electric Organ

K. FENDLER, S. JARUSCHEWSKI, A. HOBBS, W. ALBERS, and J. P. FROEHLICH

From the Max-Planck-Institute für Biophysik, D-60596 Frankfurt, Germany; National Institute on Aging, National Institutes of Health, Baltimore, Maryland 21224; and National Institute of Neurological and Communicative Disorders and Stroke, National Institutes of Health, Bethesda, Maryland 20892

ABSTRACT Time-resolved measurements of charge translocation and phosphorylation kinetics during the pre–steady state of the NaK-ATPase reaction cycle are presented. NaK-ATPase-containing microsomes prepared from the electric organ of *Electrophorus electricus* were adsorbed to planar lipid bilayers for investigation of charge translocation, while rapid acid quenching was used to study the concomitant enzymatic partial reactions involved in phosphoenzyme formation. To facilitate comparison of these data, conditions were standardized with respect to pH (6.2), ionic composition, and temperature (24°C). The different phases of the current generated by the enzyme are analyzed under various conditions and compared with the kinetics of phosphoenzyme formation. The slowest time constant ($\tau_3^{-1} \approx 8\ s^{-1}$) is related to the influence of the capacitive coupling of the adsorbed membrane fragments on the electrical signal. The relaxation time associated with the decaying phase of the electrical signal ($\tau_2^{-1} = 10–70\ s^{-1}$) depends on ATP and caged ATP concentration. It is assigned to the ATP and caged ATP binding and exchange reaction. A kinetic model is proposed that explains the behavior of the relaxation time at different ATP and caged ATP concentrations. Control measurements with the rapid mixing technique confirm this assignment. The rising phase of the electrical signal was analyzed with a kinetic model based on a condensed Albers-Post cycle. Together with kinetic information obtained from rapid mixing studies, the analysis suggests that electroneutral ATP release, ATP and caged ATP binding, and exchange and phosphorylation are followed by a fast electrogenic $E_1P \rightarrow E_2P$ transition. At 24°C and pH 6.2, the rate constant for the $E_1P \rightarrow E_2P$ transition in NaK-ATPase from eel electric organ is $\geq 1{,}000\ s^{-1}$.

INTRODUCTION

The electrogenic properties of the NaK-ATPase have been studied by a variety of techniques including the voltage clamp (Schweigert, Lafaire, and Schwarz, 1988;

Address correspondence to Dr. Klaus Fendler, Max-Planck-Institut für Biophysik, Kennedyallee 70, D-60596 Frankfurt, Germany.

J. GEN. PHYSIOL. © The Rockefeller University Press · 0022-1295/93/10/0631/36 $2.00
Volume 102 October 1993 631–666

Rakowski, Gadsby, and De Weer, 1989) and patch clamp methods (Gadsby and Nakao, 1989), potential-sensitive dyes (Clarke, Apell, and Läuger, 1989; Goldshleger, Shahak, and Karlish, 1990; Forbush and Klodos, 1991), and the bilayer technique (Fendler, Grell, Haubs, and Bamberg, 1985; Borlinghaus, Apell, and Läuger, 1987). For a review, see De Weer, Gadsby, and Rakowski (1988). The patch clamp, special voltage clamp, and bilayer techniques, as well as some potential-sensitive dyes, allow sufficient time resolution to study the electrical properties of individual partial reactions of the enzymatic reaction cycle.

In the bilayer technique, membrane fragments containing the ion pump are adsorbed to an artificial lipid bilayer. The pumps are activated by release of ATP from a photolabile protected precursor (caged ATP; Kaplan, Forbush, and Hoffman, 1978), and the capacitive current flowing across the bilayer is recorded. Analysis of the time course of the current generated by the ion pump yields information about rate constants and electrogenicity of the different partial reactions in the transport cycle. From these experiments it was concluded that the electrogenic activity of the NaK-ATPase is due to the first, Na^+-dependent steps of the reaction cycle (Fendler et al., 1985), possibly the $E_1P \rightarrow E_2P$ conformational transition (Nakao and Gadsby, 1986; Apell, Borlinghaus, and Läuger, 1987; Fendler, Grell, and Bamberg, 1987).

Correlation of the electrical and chemical events during the reaction cycle of an ion-translocating ATPase represents an important step toward the elucidation of its transport mechanism. A considerable body of evidence pertaining to the chemical properties of the intermediates of the NaK-ATPase reaction cycle has been accumulated by rapid mixing, quenched-flow techniques (Fahn, Koval, and Albers, 1966; Kanazawa, Saito, and Tonomura, 1970; Mårdh and Zetterqvist, 1974; Froehlich, Albers, Koval, Goebel, and Berman, 1976; Lowe and Smart, 1977). An especially well investigated system is the NaK-ATPase from the electric organ of the eel *Electrophorus electricus* (Fahn et al., 1966; Froehlich et al., 1976*a*). However, the electrical properties of the ion pump prepared from this tissue are largely unknown.

In this study we carried out a detailed investigation of the electrical behavior of the NaK-ATPase from eel electric organ. Time-resolved measurements allowed the investigation of charge translocation during the pre–steady state of the NaK-ATPase reaction cycle. These results were compared with rapid mixing, quenched-flow experiments, which yield kinetic information about the concomitant enzymatic partial reactions involved in phosphoenzyme formation. For a rigorous comparison of the relaxation times, parallel experiments were performed in which both techniques were applied to the same enzyme preparation under the same conditions (pH, temperature, electrolyte composition).

The objective of the comparison of time-resolved electrical and biochemical measurements was to identify the different phases of the electrical signal and to correlate them with partial reactions of the enzymatic cycle. In particular we addressed the question of the assignment and rate constant of the electrogenic step. For this purpose the interaction of the enzyme with caged ATP had to be clarified, which also proves to be important in view of previous publications using caged ATP to generate a rapid concentration jump of ATP.

MATERIALS AND METHODS

Preparation of the NaK-ATPase

Microsomal membranes containing Na,K-ATPase were prepared from the electric organ of the eel, *Electrophorus electricus* (Goldman and Albers, 1973). Samples of the material were quickly frozen and stored in liquid nitrogen before use. The activity of the enzyme, assayed by means of the coupled enzyme technique (Albers, Koval, and Siegel, 1968), was 2–3 μmol P_i/mg protein/min at 21°C.

Bilayer Measurements

Optically black lipid membranes (BLM) with an area of 0.01–0.02 cm^2 were formed in a thermostatted teflon cell as described elsewhere (Fendler et al., 1985). Each of the two compartments of the cell was filled with 1.5 ml of electrolyte containing 130 mM NaCl, 3 mM $MgCl_2$, 1 mM DTT, and 25 mM imidazole at pH 6.2. The temperature was kept at 24°C. The membrane-forming solution contained 1.5% (wt/vol) diphytanoylphosphatidylcholine (Avanti Biochemicals, Birmingham, AL) and 0.025% (wt/vol) octadecylamine (Riedel de Haen, Hannover, FRG) dissolved in *n*-decane.

The membrane was connected to an external measuring circuit via polyacrylamide gel salt bridges and Ag/AgCl or platinized Pt electrodes. The signal was amplified, filtered, and recorded with a digital oscilloscope. Usually a fourth-order, low-pass filter with a cut-off frequency of 500 Hz was used. For the investigation of the fast rise of the signal, first-order low-pass filtering with a cut-off frequency of 1 kHz was applied.

For the bilayer experiments, 15 μl of a suspension containing ~10 mg/ml protein was mixed with the same amount of a 1 mM EGTA solution and sonicated for 15 s in a bath sonicator. 15 μl of the sonicated suspension was added to one compartment of the cuvette and stirred for 30 min. Caged ATP and, if necessary, the ionophores were added under stirring to the cuvette.

To photolyse the caged ATP, light pulses of an excimer laser with a duration of 10 ns and a wavelength of 308 nm were attenuated by neutral density filters and focused onto the lipid bilayer membrane. The illuminated area of the bilayer was $\sim 7 \times 10^{-3}$ cm^2 and the energy density at the surface of the membrane was ~100 mJ/cm^2 for a release of 17% of ATP from caged ATP. After each flash, the system was kept in the dark and stirred for 10 min to allow dilution of the ATP released during the flash and its hydrolysis by the enzyme present in solution. The fraction of caged ATP converted to ATP at the membrane surface was determined in the cuvette in the absence of NaK-ATPase with a luciferin-luciferase assay (Boehringer, Mannheim, FRG) as described previously (Nagel, Fendler, Grell, and Bamberg, 1987).

The conductivity of the membrane was varied by addition of the ionophores 1799 and monensin in an ethanolic solution to both compartments. Final concentrations were 3×10^{-6} M 1799 and 3×10^{-5} M monensin. After addition of the ionophores the conductivity changed slowly over a period of 12 h. The conductivity was measured by applying a voltage of 10 mV to the membrane and measuring the induced current. At appropriate conductivity levels laser flash–induced currents were recorded.

Analysis of the Electrical Signals

The recorded signals were fitted with model functions based on two different kinetic models: (*a*) a general first-order model and (*b*) a simplified Albers-Post model. The first model has the advantage of posing no restrictions on the underlying kinetic model as long as it consists of first-order reactions. The second approach reduces the number of fit parameters and allows one to extract additional kinetic information from the current traces.

The most general case of a first-order kinetic model is a system of n intermediates, X_i, in which first-order reactions may take place between any two components. The system of differential equations describing this model can be solved by standard procedures (Benson, 1960). Assuming an arbitrary number of electrogenic steps, the current generated by this model is given by a sum of $n - 1$ exponentials plus a constant (Fahr, Länger, and Bamberg, 1981; Läuger and Apell, 1988). As discussed above, the capacitive coupling of the membrane fragments introduces an additional exponential component into the signal, the system time constant k_0^{-1} (see Appendix A). An appropriate model function for the case of the general first-order kinetic model with an arbitrary number of electrogenic steps is:

$$I(t) = \sum_{i=1}^{N} A_i e^{-t/\tau_i} + B \tag{1}$$

The amplitudes A_i, the time constants τ_i, and the stationary current B are independent fit parameters. The number N of exponential components depends on the number n of intermediates contributing to the signal and whether ($N = n$) or not ($N = n - 1$) k_0 is observed.

In the absence of ionophores the BLM is virtually nonconductive. Under these conditions the current decreases to 0 for $t \to \infty$ and the signals were analyzed with $B = 0$ in Eq. 1. Good quality fits were obtained using the automatic fit program SPLMOD (Provencher and Vogel, 1983) that requires no starting values. Each data set was fitted with the model function of Eq. 1 with N = 3–5. The solution yielding a satisfactory fit to the data with the minimum number of exponentials was used for further evaluation. In all cases, three exponential components plus (in the case of the conductivity dependence) a stationary current were sufficient to describe the data in the time range $t \geq 3$ ms. This is a rapid and convenient procedure to obtain time constants from the transient currents. As will be pointed out in the Discussion, a more detailed description of the lag and rising phases of the signal involving more than three exponential components is possible using the model described below.

A fit according to Eq. 1 has the advantage of being valid for any first-order kinetic model. (In fact, Eq. 1 does not include oscillatory behavior, i.e., complex solutions for the reciprocal time constants. This has, however, not been observed in reactions of the type discussed above [Läuger, Benz, Stark, Bamberg, Jordan, Fahr, and Brock, 1981].) A second advantage of the model function shown in Eq. 1 is that it does not require a priori knowledge about which (if any) of the exponential components is the system time constant k_0^{-1} and how many, and which, of the partial reactions are electrogenic.

The second kinetic model used for the analysis of the electrical data is a simplified Albers-Post model (Fahn et al., 1966; Post, Kume, Tobin, Orcutt, and Sen, 1969) that takes into account the activation of the enzyme by caged ATP.

$$E_1 \xrightarrow{k(t)} E_1ATP \xrightarrow{k_p} E_1P \xrightarrow{k_{12}} E_2P \xrightarrow{k_s} E_1 \tag{2}$$

This is a condensed version of the reaction scheme shown in Fig. 10, where all details not relevant to the electrical experiments have been omitted. For simplicity it is assumed that there is only a single electrogenic step involving the $E_1P \to E_2P$ transition. In addition, the following approximations are used: (*1*) All steps are irreversible. (*2*) All reactions after the electrogenic step are included in the last transition $E_2P \to E_1$. (*3*) The ATP/caged ATP binding and exchange reactions are described by a single step with an effective rate constant $k(t)$.

The justification for *3* is given in Appendix B. The release of ATP from caged ATP with the rate constant λ is described by a time-dependent fraction of released ATP $\eta(t)$:

$$\eta(t) = \eta_\infty(1 - e^{-\lambda t}) \tag{3}$$

where η_∞ refers to the released fraction of ATP after infinite time. This results in a time-dependent effective rate constant $k(t)$ according to the equation (see Eq. 11):

$$k(t) = \frac{\eta(t)}{1 - \eta(t)} k_a^+ K_{0.5}^c \tag{4}$$

The differential equations describing the model in Eq. 2 are given in Appendix C. This is not a first-order reaction sequence and the equations can only be solved numerically. The pump current of the enzyme is proportional to the time-dependent concentration of the intermediate E_1P as calculated according to the equations in Appendix C:

$$I_p(t) \propto E_1P(t) \cdot k_{12} \tag{5}$$

To account for the capacitive coupling of the ion pump via the lipid bilayer, the equivalent circuit shown in Fig. 1 has to be taken into account. The measured current $I(t)$ is calculated by solving the differential equations A2 in Appendix A. Apart from a constant scaling factor $C_m/(C_m + C_p)$, which is included in the scaling parameter of the fit, these equations depend only on k_0 and k_m. When no ionophores were present, the conductivity of the BLM was neglected ($k_m = 0$).

Each individual data set was fitted with $I(t)$ using the following variable fit parameters: the rate constants k_a^+, k_{12}, and k_s as defined in Eqs. 2 and 4, the reciprocal system time constant k_0 (Eq. A6), and a scaling parameter. The latter adjusts the absolute value of the calculated current to the experimentally determined current. Fixed values were used for the rate constant of ATP release λ and the phosphorylation rate constant k_p. As discussed above, τ_3^{-1} approximates the reciprocal system time constant k_0 in the absence of ionophores. Therefore, the starting values for k_0 in the fit were chosen so as to allow this parameter to converge to τ_3^{-1}. An example of the fit is shown in Fig. 2.

Quenched-Flow Measurements

Rapid mixing experiments were performed using a stepping motor-driven chemical quenched-flow device (Froehlich, Sullivan, and Berger, 1976*b*) equipped with Berger ball mixers (Berger, Balko, and Chapman, 1968). A circulating water bath was used for thermostating the reservoir syringes containing the enzyme and substrate solutions. Thermostating of the flow path was achieved by circulating warm air from a hair dryer over the capillary tubing and mixers. The temperature was maintained at 24°C by a feedback control circuit consisting of a thermocouple placed adjacent to the capillary tubing and connected to the hair dryer via an automated switch.

The time course of phosphoenzyme formation was measured in a medium with ionic composition identical to that used in the electrical measurements. Electric organ microsomal membranes (protein concentration, 0.66 mg/ml) suspended in 130 mM NaCl, 3 mM $MgCl_2$, 0.1 mM EDTA, 25 mM imidazole at pH 6.2, and caged ATP if required were mixed with an equal volume of an identical medium containing variable amounts of [γ^{32}P]ATP and caged ATP. After a brief time delay (2.5–300 ms) the reaction was quenched by the addition of 3% perchloric acid and 2 mM H_3PO_4 (final concentrations).

The protein in a 2-ml sample of the quenched reaction mixture was collected by centrifugation and washed three times with an ice-cold medium containing 10% polyphosphoric acid, 5% trichloroacetic acid, and 5 mM H_3PO_4. The protein was dissolved in 1 N NaOH and the radioactivity determined by counting the Cherenkov radiation in a liquid scintillation counter. A blank, prepared by acid denaturation of the enzyme before adding the [γ^{32}P]ATP, was subtracted from each sample. Protein loss occurred during the washing procedure, requiring a correction to the calculated phosphoenzyme level. To evaluate the amount of loss, a Lowry protein analysis using BSA as standard was carried out on the pellet obtained after the final

(third) wash. Protein recovery was 73.2 ± 1.4% (SEM), requiring that the phosphoenzyme level in each sample be multiplied by a factor of 1.37 to compensate for the loss during washing.

Chemicals

The protonophore 1799, 2.6-dihydroxy-1,1,1,7,7,7,-hexafluoro-2,6-bis(trifluoromethyl)-heptan-4-one, was kindly provided by Dr. P. Heytler (DuPont Co., Wilmington, DE). Monensin was a gift from Dr. G. Szabo (University of Virginia, Charlottesville, VA). Valinomycin was purchased from Serva, Heidelberg, FRG. Caged ATP was prepared as described elsewhere (Fendler et al., 1985) and kindly provided by Dr. E. Grell (MPI für Biophysik, Frankfurt, FRG). [γ^{32}P]ATP was purchased from Dupont de Nemours, Dreieich, FRG. All other reagents were of analytical or suprapure grade from Merck, Darmstadt, FRG.

RESULTS

Current Measurements

The NaK-ATPase-containing membrane fragments were adsorbed to the BLM as described in Materials and Methods. Using an inactive photolabile ATP derivative (caged ATP) a rapid ATP concentration jump can be generated by illumination of the

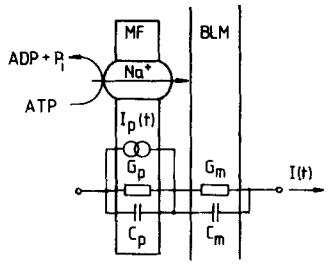

FIGURE 1. The compound membrane. NaK-ATPase-containing membrane fragments (*MF*) are adsorbed to a black lipid membrane (*BLM*). Equivalent circuit describing the coupling of the ion pump ($I_p(t)$) to the measuring circuit ($I(t)$).

compound membrane with UV laser flash. Because the release of ATP from caged ATP occurs rapidly under acidic conditions ($\tau \approx 2.5$ ms at pH 6.2, 3 mM Mg^{2+}, and 24°C; Bárabas and Keszthelyi, 1984; Walker, Reid, McCray, and Trentham, 1988), pH 6.2 was chosen to obtain a high rate of ATP release without significant loss of enzyme activity (see below). The released ATP activates the NaK-ATPase contained in the adsorbed membrane fragments and a transient current can be measured. This signal reflects charge transport during the early, Na^+-dependent steps of the reaction cycle (Fendler et al., 1985; Borlinghaus et al., 1987).

An equivalent circuit describing the electrical properties of the compound membrane is shown in Fig. 1. The current generated by the ion pump $I_p(t)$ is coupled to the measuring circuit via the capacitances and conductivities of the membrane fragments (G_p, C_p) and the BLM (G_m, C_m) and a current $I(t)$ is measured. As shown in Appendix A, the pump current is distorted by the equivalent circuit. In particular, the characteristic time constant of the compound membrane k_0^{-1} is introduced into the signal.

Fig. 2 shows the electrical current measured after photolytic release of ATP from caged ATP. In the absence of an appropriate ionophore, the conductivity G_m of the

BLM is neglegible. Consequently, the pump current of the NaK-ATPase is capacitively coupled to the measuring system via the capacitance of the BLM. Under these conditions the electrical current measured after the photolytic release of ATP is characterized by three phases: a rapid rise (τ_1^{-1} = 200–300 s^{-1}), a slower decay ($\tau_2^{-1} \approx 40\ s^{-1}$), and a very slow component with negative amplitude ($\tau_3^{-1} \approx 8\ s^{-1}$). The numbers characterizing the three components refer to the conditions of experiment 1 in Fig. 2 (130 mM NaCl, 3 mM $MgCl_2$, 1 mM DTT, and 25 mM imidazole at pH 6.2).

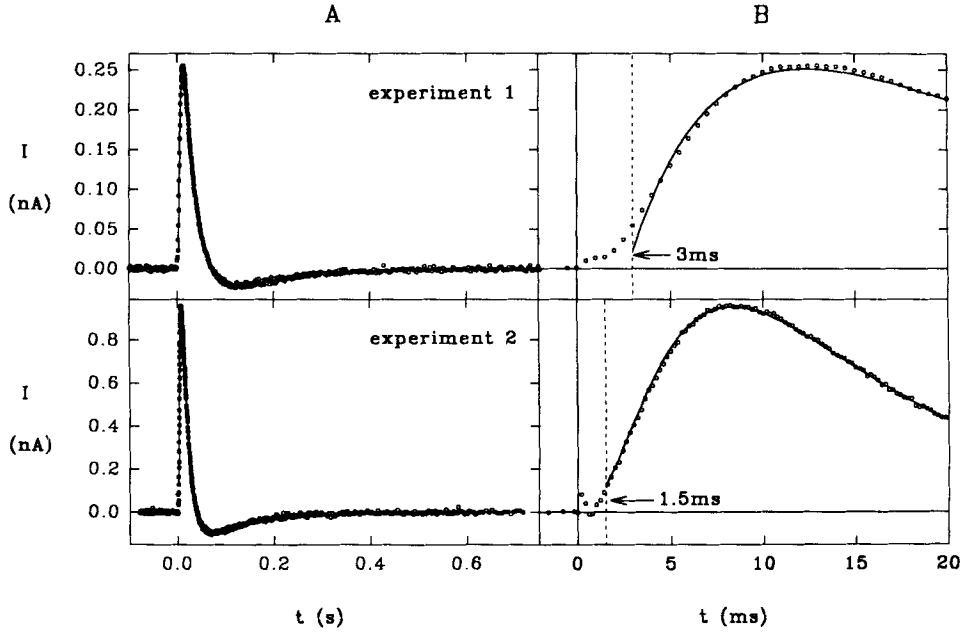

FIGURE 2. (A) Electrical current measured after release of ATP by a UV laser flash. Caged ATP concentrations before the UV flash and the fraction of released ATP, η, were: 100 μM and 0.11 (experiment 1) and 300 μM and 0.20 (experiment 2). The solid line is a fit to the data according to two different model functions. Experiment 1: a general first-order reaction cycle (Eq. 1) with the parameters τ_i = 204, 37, and 7.9 s^{-1}; A_i = −0.83, 0.61, and −0.073 nA; and B = 0. Experiment 2: a condensed Albers-Post scheme (Eq. 2) with the parameters λ = 407 s^{-1}, $k_a^+ = 8.4 \times 10^6\ s^{-1}\ M^{-1}$, k_p = 450 s^{-1}, k_{12} = 2,900 s^{-1}, k_s = 1.5 s^{-1}, k_0 = 9.7 s^{-1}. (B) Data of A shown on an expanded scale.

Two different experiments are shown in Fig. 2. Experiment 1 is the control for the phosphorylation measurement shown in Fig. 8. It was performed with the same enzyme preparation, and the caged ATP concentration (100 μM) and fraction of released ATP (η = 0.11) were chosen to approximate the conditions of the phosphorylation experiment. Because in this comparison the slow decay of the signal is important, the current was recorded using the 500 Hz fourth-order low-pass filter. Experiment 2 was designed to analyze the fast rise of the signal. It was therefore

performed using the 1 kHz first-order low-pass filter and a high caged ATP concentration (300 μM) and fraction of released ATP ($\eta = 0.20$).

Illumination of the membrane with UV light and the photolytic reaction cause an artefact, distorting the electrical signal immediately after the light flash (see Fig. 2 and Fendler et al., 1987). Therefore, only data sampled at $t > 3$ ms (experiment 1) and $t > 1.5$ ms (experiment 2) were used for the analysis. In experiment 2, the time range not used for the analysis was shorter since fast recording accelerates the decay of the artefact.

Fig. 2 also shows examples of the two different model functions used in the analysis of the data (solid lines). Experiment 1 was fitted with a general first-order model (Eq. 1), while for experiment 2 a modified Albers-Post model (Eq. 2) was applied. Parameters obtained from these fits are given in Table II. The parameters in the table are average values from fits to several different recordings obtained under the same conditions. Experiments 1 and 2 refer to the current traces shown in Fig. 2, which represent one of the data sets used for curve fitting. The modified Albers-Post model was appropriate for experiment 2 since it allows one to analyze the fast rise of the signal in greater detail (see below).

One of the objectives in this study was to discriminate charge transport by the NaK-ATPase from the system time constant k_0^{-1} and to assign the different phases of the signal to processes in the reaction cycle of the enzyme. Therefore, the signal was recorded under a variety of conditions. In a second set of experiments, these data were compared with results obtained by rapid mixing, quenched-flow studies (see below). This allowed direct comparison of chemical and electrical processes in the reaction cycle of the enzyme.

Time Constants of the Electrical Signal under Different Conditions

In this section, results from the electrical experiments conducted under various conditions are reported. Unless otherwise stated, the reciprocal relaxation time constants τ_i^{-1}, amplitudes A_i, and the stationary current B describing the current traces were determined by the fitting procedure based on the general first-order model (Eq. 1). In all cases, with the exception of experiments addressing the conductivity dependence, B was set to 0.

Each of the experiments shown in Figs. 3, 4, 6, and 7 was performed using a single membrane, while the conductivity of the membrane, temperature, caged ATP concentration, or the fraction η of release ATP were changed. These experiments lasted several hours and involved up to 50 UV flashes. As reported previously, no inactivation of the enzyme during the measurement was observed (Fendler et al., 1985).

Using a combination of the UV light–insensitive protonophore 1799 and the Na^+/H^+ exchanger monensin (together a Na^+ conducting system), the conductivity of the membrane fragments and the lipid bilayer can be varied. This approach was used to investigate the effect of the capacitive coupling (Fig. 1) on the current generated by the NaK-ATPase and to identify the system time constant k_0^{-1}.

In Fig. 3, the parameters of the signal are plotted versus the membrane conductivity. This value represents the combined conductivities of the bilayer and the adsorbed membrane fragments. To estimate the contributions of the different components of

the compound membrane to the measured conductivity, information pertaining to the coverage of the BLM with membrane fragments is required. Although the shape of the signal was always the same under identical conditions, the magnitude of the peak current varied considerably. We attribute this effect to a variable density of membrane fragments adsorbed to the BLM. While the peak current could be as high as 130 nA/cm^2 in some experiments (Fig. 2), the peak current in the case of the conductivity dependence (Fig. 3) was only ~18 nA/cm^2. From this we conclude that

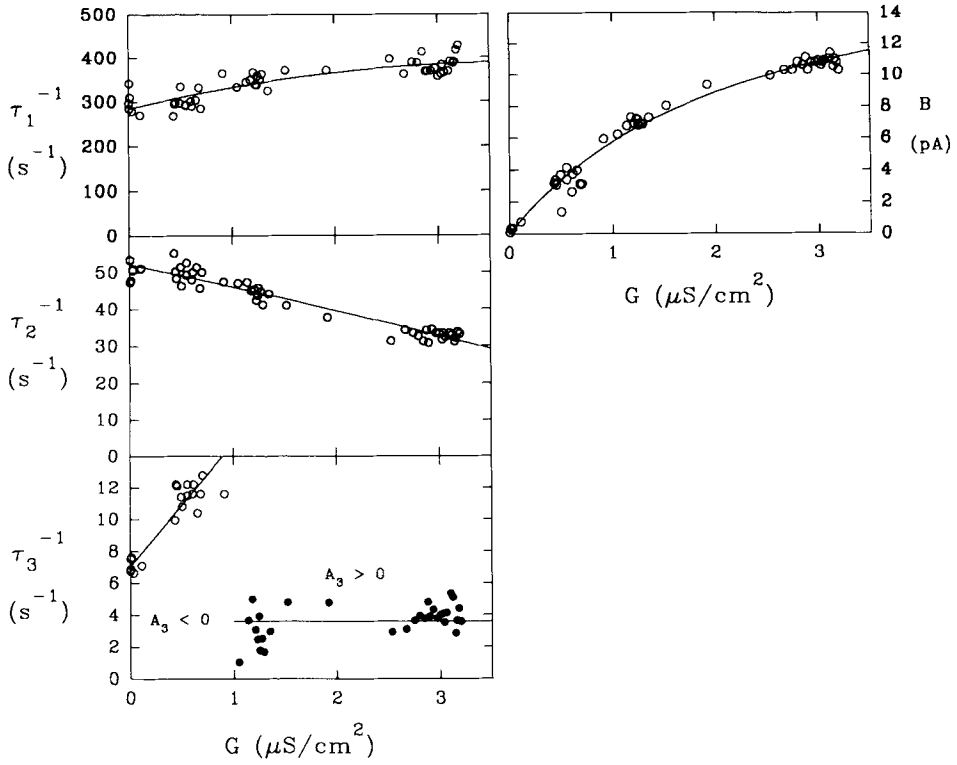

FIGURE 3. Reciprocal time constants τ_i^{-1} and stationary current B at different conductivities of the compound membrane. The caged ATP concentration before the UV flash was 600 μM with a fraction of released ATP of η = 0.15. The conductivity was varied by addition of the ionophores 1799 and monensin. The parameters τ_i and B were determined from a fit according to the general first-order model (Eq. 1) with N = 3. The solid lines are guides to the eye.

during this experiment only a small part of the BLM was covered with membrane fragments and that the measured conductivity is approximately equal to the conductivity of the bilayer G_m.

The reciprocal time constants and the stationary current at different conductivities are plotted in Fig. 3. The caged ATP concentration in this experiment was 600 μM and the fraction of released ATP was η = 0.15. While τ_1^{-1} and τ_2^{-1} change smoothly, with conductivity showing a saturating behavior, τ_3^{-1} doubles at low conductivities and

the corresponding amplitude changes sign at $G \approx 1$ μS/cm^2. The fact that the largest changes in amplitude and time constant are observed for τ_3 may be taken as an indication that this time constant corresponds to the system time constant k_0^{-1}.

Fig. 4 illustrates the temperature dependence of the time constants corresponding to the different phases of the electrical signal. They were determined at temperatures between 5 and 24°C with a caged ATP concentration of 1 mM and a fraction of released ATP of $\eta = 0.21$. Linear Arrhenius plots were obtained over the entire temperature range. The activation energies determined for τ_1, τ_2, and τ_3 were 101, 68, and 86 kJ/mol, respectively. These values are characteristic of protein-dependent reactions. No activation energy indicative of a simple diffusion process (e.g., Na^+ in water: 15 kJ/mol) expected for the system time constant was found.

Caged ATP has been shown to be a competitive inhibitor of the NaK-ATPase (Forbush, 1984; Nagel et al., 1987). To investigate the effect of caged ATP on the

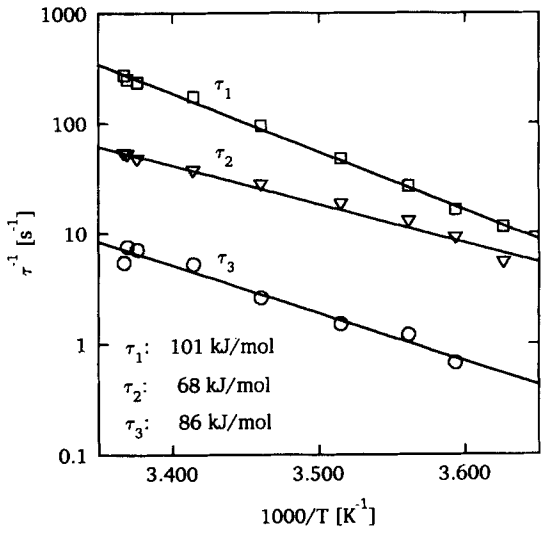

FIGURE 4. Arrhenius plot of the reciprocal time constants τ_i^{-1}. The caged ATP concentration before the UV flash was 1 mM with a fraction of released ATP of $\eta = 0.21$. The time constants τ_i were determined from a fit according to the general first-order model (Eq. 1) with $N = 3$ and $B = 0$. The activation energies were calculated from the slope of the regression lines shown in the figure.

enzyme, signals were recorded at different ATP concentrations or at different ATP/caged ATP ratios. The ATP/caged ATP ratio was varied by applying different UV laser energies to the membrane. This results in a variable fraction η of caged ATP being transformed to ATP.

In Fig. 5, the electrical signal is shown at three different caged ATP concentrations (before the UV flash). In this experiment, the concentration of ATP (and caged ATP) after the UV flash was varied by adding different amounts of caged ATP to the electrolyte while maintaining the laser energy constant. This resulted in a constant fraction ($\eta = 0.23$) of released ATP. The influence of ATP (and caged ATP) on the decay of the signal is immediately apparent, while the rising phase remains unaffected. To estimate the quality of the fits, the residuals are included in Fig. 5.

The reciprocal time constants τ_1^{-1}, τ_2^{-1}, and τ_3^{-1} obtained by the fit at different caged ATP concentrations are shown in Fig. 6. Only τ_2^{-1} and τ_3^{-1} are dependent on

the concentration of caged ATP. In contrast, τ_1^{-1} is independent of the caged ATP concentration. The dependence of τ_2^{-1} on the concentration before the flash of caged ATP follows a hyperbolic saturation dependence. A fit with a function of this type is included in the figure yielding a half-saturation concentration of 46 μM caged ATP. Also included in the figure is the peak current I_{max}. The concentration dependence of I_{max} is similar to that of τ_2^{-1} with a half-saturation concentration of 57 μM and a

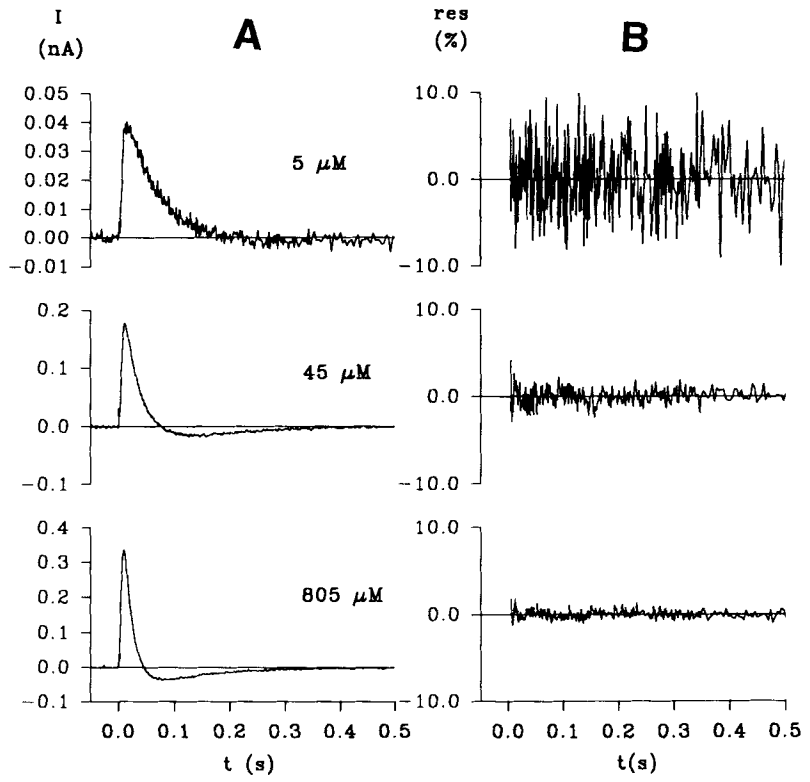

FIGURE 5. (A) Effect of varying caged ATP concentrations and a constant fraction $\eta = 0.23$ of released ATP on the electrical signal. In the figure the caged ATP concentration before the UV flash is given. Conditions are as described in Materials and Methods. (B) Residuals of a fit to the data of A according to the general first-order model (Eq. 1) with $N = 3$ and $B = 0$. The residuals are given as a fraction (in %) of the maximal current of the corresponding current trace.

maximum value of 390 pA. For comparison, I_{max} and τ_2^{-1} were scaled so as to have the same maximum values on the graph.

At low caged ATP concentrations ($c_c^0 \leq 25$ μM), τ_3^{-1} also decreases. Under these conditions, the caged ATP-dependent process (described by τ_2 at $c_c^0 > 25$ μM) becomes slower than the caged ATP-independent one (described by τ_3 at $c_c^0 > 25$ μM). The relaxation times τ_2 and τ_3 change meaning, or, in other words, the

dependence of τ_3 on caged ATP concentration results exclusively from the fact that the time constants are assigned to specific phases of the signal rather than to specific underlying processes. In the following, all assignments of molecular processes to phases of the electrical signal refer to high caged ATP conditions ($c_c^0 > 25$ μM). Also, there seems to be a slight decrease of τ_1^{-1} at low caged ATP concentrations. However, in this region the signal to noise ratio is already poor (Fig. 5) and the effect may be due to a fit artefact.

According to the model proposed in the discussion section for ATP and caged ATP binding and exchange, the maximal value of τ_2^{-1} is expected to vary with the fraction η of released ATP (see Eq. 11). Therefore the signal was recorded at saturating caged

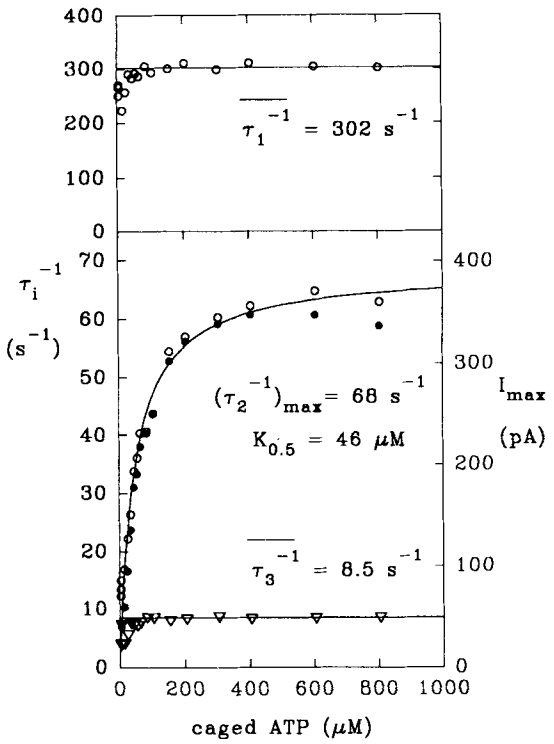

FIGURE 6. Time constants τ_i (○, ▽) and peak current I_{max} (●) at different concentrations of caged ATP and $\eta = 0.23$. In the figure the caged ATP concentration before the UV flash is given. Typical current traces of this experiment are shown in Fig. 5. The parameters τ_i were determined from a fit according to the general first-order model (Eq. 1) with $N = 3$ and $B = 0$. The horizontal lines are drawn at the average values of τ_1^{-1} and τ_3^{-1} for $c_c^0 \geq 100$ μM, where c_c^0 is the concentration of caged ATP before the UV flash. The curved solid line is a fit to the data with a hyperbolic saturation dependence $\tau_2^{-1} = (\tau_2^{-1})_{max}\, c_c^0/(c_c^0 + K_{0.5})$.

ATP concentration (300 μM) and different laser intensities corresponding to different amounts of released ATP. For comparison with the theoretical prediction (see Eq. 11 in the Discussion) the reciprocal time constant τ_2^{-1} is plotted versus $\eta/(1 - \eta)$ (Fig. 7).

One of the assumptions involved in modeling the data with Eq. 2 merits further consideration. The approximative description of the interaction of the enzyme with ATP and caged ATP by Eqs. 2–4 and C1 (Appendix C) is only valid if all of the protein starts in the intermediate E_1cagedATP and proceeds via E_1 to E_1ATP (see Eq. 8). Since the model was only applied to data obtained at high caged ATP concentrations, this prerequisite is met. However, after the UV flash two populations of enzyme

are present: one activated by ATP released in the ATP binding site and one that binds ATP released in solution. We tested this mechanism by simulating the electrical signal with a model including the release of caged ATP in solution as well as release in the binding site. The latter leads to a rapid phosphorylation of the enzyme, thereby virtually eliminating the lag phase in the simulated electrical signal. This is contradictory to the experimentally obtained signal, which shows a lag phase of several milliseconds. Therefore, release of ATP in the binding site of the protein was excluded.

Rapid Mixing, Quenched-Flow Experiments

With [γ^{32}P]ATP as substrate, rapid mixing, quenched-flow experiments were performed to correlate charge translocation measured with the bilayer technique to the kinetics of phosphoenzyme formation. In parallel with some of the phosphorylation measurements, an electrical control experiment was performed using the same enzyme preparation. Care was taken to match temperature and electrolyte composition in both measurements as closely as possible.

To test the competitive influence of caged ATP, quenched-flow measurements were

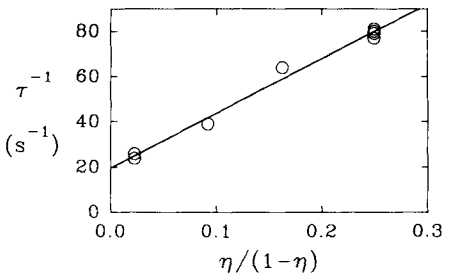

FIGURE 7. Dependence of τ_2^{-1} on the fraction η of released ATP. The concentration of caged ATP before the UV flash was 300 μM. τ_2^{-1} was determined from a fit according to the general first-order model (Eq. 1) with $N = 3$ and $B = 0$. The solid line is a linear regression line to the data with slope 240 s^{-1} and τ_2^{-1} ($\eta = 0$) = 20 s^{-1}.

carried out in the absence and presence of caged ATP in conjunction with a parallel electrical experiment (Fig. 2, experiment 1). The extent of conversion of caged ATP to ATP in the electrical measurement was determined with the luciferin/luciferase assay. Using these data, the concentrations of ATP and caged ATP were adjusted to the same level in the quenched-flow and the electrical experiments. The results of the electrical measurements are summarized in Table II.

For the experiment in the absence of caged ATP, electric organ microsomes were suspended in standard buffer solution (130 mM NaCl, 3 mM $MgCl_2$, 0.1 mM EDTA, and 25 mM imidazole at pH 6.2) and mixed with the same amount of buffer containing 20 μM [γ^{32}P]ATP. This corresponds to an initial concentration of [γ^{32}P]ATP in the reaction medium of 10 μM. After a predetermined time the amount of phosphoenzyme formed was measured by quenching with strong acid. The experiment in the presence of caged ATP was performed in an analogous manner. Microsomes in standard buffer containing 100 μM caged ATP were mixed with an equal volume of substrate medium containing 20 μM [γ^{32}P]ATP and 80 μM caged ATP. The concentrations of [γ^{32}P]ATP and caged ATP after mixing were 10 and 90

μM, respectively. These conditions correspond to a 10% release of ATP from caged ATP and thus approximate the substrate levels present in the laser flash experiments.

In Fig. 8, the time course of phosphoenzyme formation at 24°C with (filled symbols) and without (open symbols) caged ATP is shown. Two different experiments, each in the presence and absence of caged ATP and using the same enzyme preparation, were performed under identical conditions. The first experiment spans the time range 0–100 ms and the second the range 0–200 ms. All data points were normalized to the maximal phosphoenzyme level, EP_{max}. EP_{max} was calculated as the average of all data points with $t \geq 75$ ms for the first, and $t \geq 100$ ms for the second experiment. Experimental values determined in the presence and absence of caged ATP were used together to calculate a separate EP_{max} for each experiment.

The rate constant for phosphoenzyme formation was calculated on the basis of the kinetic model:

$$E \xrightarrow{\tilde{k}_a^+} EATP \xrightarrow{k_p} EP \qquad (6)$$

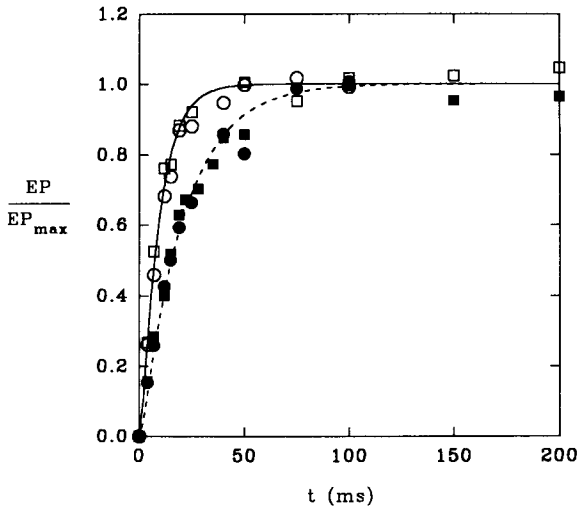

FIGURE 8. Phosphoenzyme formation in the presence (*filled symbols*) and absence (*open symbols*) of caged ATP. The results of two identical experiments are shown. Experiment 1 (*circles*): EP_{max} = 0.73 nmol·mg^{-1}; experiment 2 (*squares*): EP_{max} = 0.89 nmol·mg^{-1}. Concentrations of nucleotides after mixing: 10 μM [γ^{32}P]ATP and 90 μM caged ATP (*open symbols*), only 10 μM [γ^{32}P]ATP (*filled symbols*). For comparison, the result of a kinetic model as described in the text is included (*solid and dashed lines*).

where $\tilde{k}_a^+$ represents the pseudo-monomolecular rate constant for ATP binding and k_p the phosphorylation rate constant.

Here and in Eq. 7, ATP dissociation (k_a^-) was neglected because $k_p \gg k_a^-$. To test whether this assumption is valid, the rate constant for ATP dissociation was measured under the conditions of our experiments (24°C, pH 6.2, electrolyte composition as described in Materials and Methods). A rapid mixing technique as described by Froehlich, Hobbs, and Albers (1983) was used (data not shown), yielding a rate constant of k_a^- = 94 s^{-1}. This is approximately two times larger than the value obtained before at 21°C and pH 7.5 (k_a^- = 42 s^{-1}; Froehlich et al., 1983). Comparison with the rate constant for phosphorylation, $k_p \approx 450$ s^{-1} (Table II), shows that ATP dissociation can indeed be neglected in the kinetic models.

Good agreement of the model in Eq. 6 with the data was obtained with the

following values for the rate constants: $k_p = 450\ s^{-1}$, and (*a*) in the absence of caged ATP, $\tilde{k}_a^+ = 120\ s^{-1}$ (solid line); (*b*) in the presence of caged ATP, $\tilde{k}_a^+ = 50\ s^{-1}$ (dashed line). The slower rise of the phosphoenzyme concentration in the presence of caged ATP demonstrates the inhibitory effect of caged ATP on ATP binding. This is also reflected in the lower value obtained for the apparent ATP binding rate constant under these conditions.

The ATP/caged ATP exchange reaction is dependent on the caged ATP dissociation rate constant, k_c^- (see Eq. 9). Therefore an attempt was made to measure the dissociation of caged ATP from the NaK-ATPase using the rapid mixing technique. After incubation with 100 μM caged ATP, the enzyme was diluted 20-fold into 100

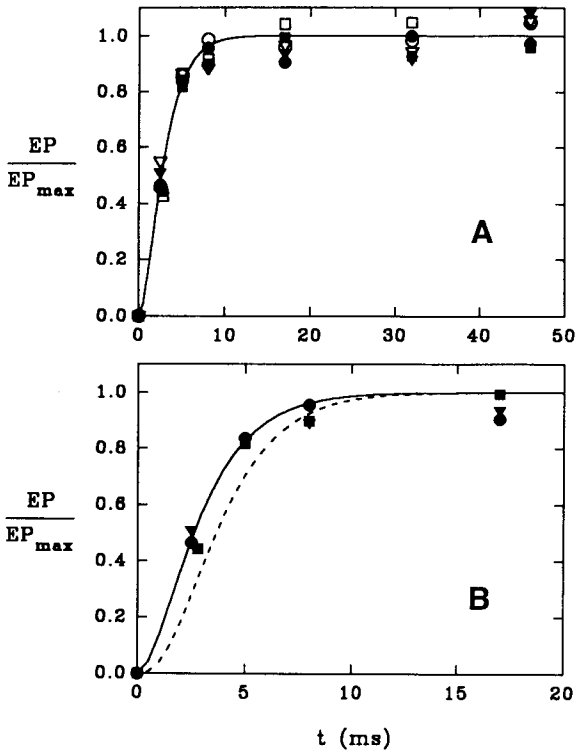

FIGURE 9. Dissociation rate constant of caged ATP. Dilution and phosphorylation with 100 μM [γ^{32}P]ATP without preincubation (*open symbols*) or after preincubation with 100 μM caged ATP (*filled symbols*). The results of three identical experiments are shown. Experiment 1 (*circles*): EP_{max} = 0.37 nmol·mg^{-1}; experiment 2 (*triangles*): EP_{max} = 0.76 nmol·mg^{-1}; experiment 3 (*squares*): EP_{max} = 0.17 nmol·mg^{-1}. In B, the data obtained in the presence of caged ATP are shown on an expanded time scale. The lines given in the figure are calculated according to two different kinetic models described in the text.

μM [γ^{32}P]ATP. At 100 μM caged ATP, the fraction of enzyme containing bound caged ATP is 75%, but declines to ~13% after dilution of the caged ATP to 5 μM (calculated with a binding constant for caged ATP of $K_{0.5}^c$ = 35 μM; see Discussion). This means that the majority of the enzyme will be available for rapid phosphorylation only after caged ATP has dissociated from the binding sites. Under these conditions, the formation of the phosphoenzyme will be delayed by the rate of dissociation of caged ATP. For a control, a separate dilution and phosphorylation experiment was performed under identical conditions and using the same enzyme preparation. However, no caged ATP was present in the solution during this experiment.

The time course of EP formation after caged ATP preincubation (filled symbols) together with the control experiment (open symbols) is shown in Fig. 9. The figure summarizes the results of three different experiments performed under identical conditions, together with their respective controls. For each experiment and its control, the same enzyme preparation was used and the measurements were normalized as described in Fig. 8. EP_{max}, calculated as the average of the data points measured at $t \geq 17$ ms, showed considerable variation (0.17–0.76 nmol · mg^{-1} protein); however, the apparent rate constant of EP formation remained fairly constant, as demonstrated by the overlap in the transient time courses. Comparison of the control and caged ATP preincubation experiments shows that the two time courses are virtually indistinguishable. This demonstrates that the dissociation of caged ATP is not rate limiting under the conditions of the experiment.

The solid line shown in Fig. 9 describes the formation of the phosphoenzyme in the absence of caged ATP according to the kinetic model in Eq. 6 with $k_p = 450\ s^{-1}$ and $\tilde{k}_a^+ = 1{,}200\ s^{-1}$ ($\tilde{k}_a^+ = k_a^+ \cdot c_a$, where $k_a^+ = 1.2 \cdot 10^7\ M^{-1}s^{-1}$ is the second-order rate constant for ATP binding and $c_a = 100\ \mu M$ is the ATP concentration). The same simulation together with the data obtained after caged ATP preincubation are shown on an expanded scale in Fig. 9 B. Also shown (dashed line) is a simulation corresponding to a kinetic model that includes the caged ATP dissociation step.

$$\text{EcagedATP} \xrightarrow{k_c^-} \text{E} \xrightarrow{\tilde{k}_a^+} \text{EATP} \xrightarrow{k_p} \text{EP} \qquad (7)$$

The rate constants were identical to those used in the previous case and, in addition, $k_c^- = 1{,}000\ s^{-1}$. The latter was chosen as an approximation to the lower limit for the rate of caged ATP dissociation. The calculated curve clearly rises too slowly to explain the experimental data indicating that the rate constant for caged ATP dissociation in eel electric organ NaK-ATPase is 1,000 s^{-1} or greater at 24°C.

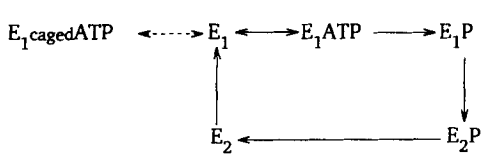

FIGURE 10. Reaction sequence of the NaK-ATPase. In the case of the electrical experiments where caged ATP was present, the binding and dissociation of caged ATP also has to be taken into account (*dashed arrows*).

DISCUSSION

To gain insight into the transport mechanism of ion translocating enzymes, we must understand how changes in the chemical state of the enzyme such as phosphorylation, conformational transitions, or substrate binding bring about the transport of ions. We, therefore, have combined a method that yields information about translocated charge with a technique sensitive to the chemistry of the enzyme: bilayer electrical measurements and rapid acid quenching.

The current reaction model for the NaK-ATPase is the Albers-Post scheme (Fahn et al., 1966; Post et al., 1969). Fig. 10 shows this scheme, which has been modified to include caged ATP binding to the enzyme. For a comparison with the electrical measurements, the rate constants of the different partial reactions in this model were

taken from the literature or determined with the rapid mixing, quenched-flow method under identical conditions.

For the analysis of the electrical signal, it is important to take into account the distortion of the signal by the measuring circuit. Therefore, in the first section we address the question of which, if any, of the observed time constants corresponds to the system time constant τ_0 ($=k_0^{-1}$), the characteristic time constant of the compound membrane. In the following sections the rising and decaying phases of the electrical signal are correlated with partial reactions of the Albers-Post cycle. From this we determine the assignment and rate constant of the electrogenic step. The rate constant of the electrogenic step is compared with values available in the literature and reasons for the existing discrepancies are discussed.

The System Time Constant

The NaK-ATPase-containing membrane fragments are capacitively coupled to the measuring circuit via the BLM. The electrical properties of the system are described by the equivalent circuit shown in Fig. 1. As shown in Appendix A, the system time constant τ_0 ($=k_0^{-1}$) is introduced into the signal. In the absence of ionophores (conductivity of the BLM, $G_m \approx 0$) the system time constant is determined by C_p and C_m, the capacitances of the membrane fragments and the underlying bilayer, and the conductivity of the membrane fragments G_p: $\tau_0 = k_0^{-1} = (C_m + C_p)/G_p$. The conductivity G_p includes all possible pathways for flow of charge from the interstitial space between the extracellular face of the membrane fragments and the BLM to their intracellular side. This could be the conductivity of the membrane fragments, leakage through the cleft between membrane fragments and BLM, or a leak through the protein itself.

The current generated by the ion pump can be reconstructed from the recorded current as described in Appendix A. This calculation requires the knowledge of k_0 (in the absence of ionophores $k_m = 0$). In addition, τ_0 ($=k_0^{-1}$) is introduced into the signal and has to be discriminated from relaxation time constants associated with the catalytic activity of the enzyme. All of this emphasizes the importance of identifying the system time constant in the measured signal.

The slowest exponential component observed in the electrical signals generated by the NaK-ATPase from mammalian kidney on lipid bilayers has been previously been assigned to the system time constant (Borlinghaus et al., 1987; Fendler et al., 1987). In the case of bacteriorhodopsin-containing purple membranes attached to lipid bilayers, a similar system time constant was found ($\tau \approx 200$ ms; Bamberg, Apell, Dencher, Sperling, Stieve, and Läuger, 1979). It therefore seemed reasonable to assign $\tau_3 \sim 130$ ms observed in the eel preparation to the system time constant. There are, however, several problems associated with that assignment:

(*1*) As reported previously (Fendler et al., 1987), the system time constant measured with membrane fragments from pig kidney is larger in the presence of K^+ (~ 500 ms) than in the absence of K^+ (~ 200 ms). However, in the presence of K^+, the stationary current generated by the ion pump is higher (Nagel et al., 1987) and the capacitances of BLM and membrane fragments should be charged more rapidly (Bamberg et al., 1979). Therefore, in contrast to experimental observations, a smaller rather than a larger system time constant is expected in the presence of K^+.

(2) The strong temperature dependence of τ_3^{-1} with an activation energy of 86 kJ/mol (Fig. 4) is difficult to explain since k_0 only depends on the conductivities and capacitances of the compound membrane. For bacteriorhodopsin-containing purple membranes adsorbed to a lipid bilayer, an activation energy of the system time constant of only 20 kJ/mol was reported (Holz, 1990).

In view of these difficulties, it was important to test whether the assignment of τ_3 to the system time constant is correct. Since the system time constant k_0^{-1} should depend on the conductivities G_m and G_p as described in Appendix A, the signal was investigated at different levels of the permeability G of the membrane.

As the conductivity increases from 0 to 1 $\mu S/cm^2$, τ_3^{-1} rises from 7 to 12 s^{-1} (Fig. 3). An increase of k_o with increasing conductivities G_m and G_p is consistent with Eq. A6. In addition, the amplitude for τ_3 drops to 0 at $G = 1$ $\mu S/cm^2$ because, with increasing G_m, k_m approaches k_o and a_o vanishes (see Eq. A5). This behavior supports the concept that τ_3 is the time constant of the membrane system and corresponds to the discharging of C_m and C_p via G_m and G_p.

At $G > 1$ $\mu S/cm^2$, a new component with $\tau_3^{-1} = 4$ s^{-1} and a positive amplitude appears (Fig. 3). Indeed, the reappearance of the system time constant with an amplitude of opposite sign is to be expected at increasing conductivities (see Eq. A5). However, k_o should be larger than at low conductivities (see Eq. A6), which is not the case for τ_3^{-1}.

The unexplained behavior of τ_3 at $G > 1$ $\mu S/cm^2$ and its large temperature dependence at $G = 0$ cannot be explained on the basis of a diffusion controlled leakage out of the interstitial space between membrane fragments and BLM, but instead seems to argue for an involvement of the protein in this time constant. Possibly, the slow reciprocal time constant of 4 s^{-1} represents a time constant for the pump current $I_p(t)$ of the enzyme and is also present in the absence of ionophores, but is masked by the system time constant. With increasing conductivities and the concomitant increase in k_0, the time constants become separated and $\tau_3^{-1} = 4$ s^{-1} appears. Another possibility for this behavior is a protein-mediated backflow of charge across the membrane fragments. This would account for the high activation energy of τ_3 and explain why the description of the compound membrane in terms of purely electrical quantities is not valid.

In both cases, the behavior of τ_3 in the absence of ionophores ($\sim$130 ms) is dominated by a discharge mechanism possibly involving the protein. Therefore, it can be assigned to the system time constant k_0^{-1}, which yields a consistent qualitative description of the behavior of τ_3. The extent of the involvement of the protein cannot be estimated at present. However, this does not affect the discussion of the remaining time constants τ_1 and τ_2 as long as τ_3 approximates the real value of the system time constant.

In the following, the time constants τ_1 and τ_2 of the rising and decaying phases of the signal will be assigned to the enzymatic activity of the NaK-ATPase. As shown in Fig. 3, these time constants are only slightly dependent on the conductivity of the membrane. This indicates that no significant potential across the membrane fragments is generated by the pump or that its influence on the kinetics of the

NaK-ATPase is neglegible. A similar conclusion has been drawn by Borlinghaus et al. (1987) and Nagel et al. (1987).

The Decaying Phase of the Signal: ATP and Caged ATP Binding

In contrast to τ_3, τ_1 and τ_2 are only slightly affected by ionic gradients or potentials built up across the NaK-ATPase-containing membrane fragments. This is demonstrated by their near independence of the conductivity of the membranes (see Fig. 3). For NaK-ATPase from mammalian kidney it has been proposed that these time constants are due to the pumping activity of the enzyme (Borlinghaus et al., 1987; Fendler et al., 1987).

It has been reported previously (Fendler et al., 1987) for the NaK-ATPase from pig kidney that only the time constant for the decay of the electric signal depends on the caged ATP concentration. It was also shown that caged ATP binds to the NaK-ATPase, although with a somewhat lower affinity than ATP (Forbush, 1984). These findings led to the conclusion that τ_2^{-1} corresponds to ATP released after a UV flash, binding to the enzyme and exchanging for the caged ATP already bound.

A similar observation is made for the NaK-ATPase from eel electric organ: τ_2^{-1} saturates under the conditions of Fig. 6 at 68 s^{-1}. In contrast to steady-state enzymatic behavior, the reciprocal time constant associated with substrate binding is not expected to saturate, but rather to increase linearly with increasing substrate concentration until it is rate limited by a subsequent reaction. As shown in the next sections, all rate constants after substrate binding are on the order of ~ 500 s^{-1} and therefore cannot account for the saturation of τ_2^{-1} at 68 s^{-1}.

In the following, a model is discussed that explains the hyperbolic ATP dependence of τ_2^{-1} in the presence of caged ATP. It is assumed that ATP and caged ATP bind to the enzyme in the E_1 conformation. Only protein with ATP in its binding site can then be phosphorylated and proceed in the reaction cycle.

Since the rate constant for the phosphorylation reaction ($k_p \approx 450$ s^{-1}; see Table II) is much larger than the ATP dissociation rate constant ($k_a^- = 94$ s^{-1}; see Results), the ATP dissociation reaction can be neglected and the following simplified kinetic model describes the interaction of the enzyme with ATP and caged ATP:

$$E_1\text{cagedATP} \underset{\tilde{k}_c^+}{\overset{k_c^-}{\rightleftharpoons}} E_1 \xrightarrow{\tilde{k}_a^+} E_1\text{ATP} \tag{8}$$

k_c^- is the caged ATP dissociation rate constant and $\tilde{k}_c^+ = (1 - \eta)\, c_c^0 k_c^+$ and $\tilde{k}_a^+ = \eta c_c^0\, k_a^+$ are the pseudo-monomolecular binding rate constants for caged ATP and ATP, respectively. The pseudo-monomolecular binding rate constants depend on the concentration c_c^0 of caged ATP before the flash, the fraction η of released ATP, and the second-order binding rate constants, k_c^+ and k_a^+, of the nucleotides. As mentioned above, the formation of E_1ATP is virtually irreversible. Also, under K^+-free conditions, the decay of the phosphointermediates is very slow. Therefore, formation of E_1 due to enzyme cycling is comparatively slow and to a first approximation the interaction of the enzyme with ATP and caged ATP can be treated separately as described by the reaction sequence 8.

In Appendix B, the reciprocal time constant describing ATP and caged ATP

binding and exchange is calculated (Eq. B1). Following these results the dependence of τ_2^{-1} on the caged ATP concentration c_c^0 and on the fraction η of released ATP can be written as:

$$\tau_2^{-1} = \eta k_a^+ K_{0.5} \frac{c_c^0}{c_c^0 + K_{0.5}} \tag{9}$$

with

$$K_{0.5} = \frac{k_c^-}{(1 - \eta)k_c^+ + \eta k_a^+}$$

For a constant fraction η of released ATP this is a hyperbolic dependence with respect to the caged ATP concentration. In the experiments this behavior was, in fact, observed for τ_2^{-1} (see Fig. 6). The agreement between the experimental data and the predicted hyperbolic concentration dependence of τ_2^{-1} suggests that the interpretation of τ_2 as the time constant describing caged ATP and ATP binding and exchange is correct.

Except at very low caged ATP concentrations, the reciprocal time constant for the decaying phase τ_2^{-1} is much larger than the reciprocal system time constant, τ_0^{-1} ($= \tau_3^{-1}$; see preceeding section). Under these conditions, and because $\tau_1^{-1} \gg \tau_2^{-1}$, the integral of the pump current, i.e., the charge transported per cycle, is approximately proportional to the product $I_{max} \cdot \tau_2$. This product is constant for different caged ATP concentrations as demonstrated by the nearly identical caged ATP dependence of I_{max} and τ_2^{-1} in Fig. 6. A constant charge per cycle is indeed exspected for the NaK-ATPase at different caged ATP concentrations and is consistent with the kinetic models in Eqs. 2 and 8. Hence, in addition to the time constants, the amplitudes of the electrical signal conform to the kinetic models used for the analysis.

From Eqs. 9 the ATP binding rate constant k_a^+ and the caged ATP binding constant $K_{0.5}^c$ can be expressed as functions of the phenomenological parameters $(\tau_2^{-1})_{max}$ and $K_{0.5}$. For $\eta \ll 1$ $(\tau_2^{-1})_{max}$ is much larger than the rate constant of caged ATP dissociation k_c^- ($k_c^- > 1{,}000\ s^{-1}$; see Results) and the following approximate relations can be calculated:

$$k_a^+ = \frac{(\tau_2^{-1})_{max}}{\eta K_{0.5}}$$

and

$$K_{0.5}^c = (1 - \eta)K_{0.5} \tag{10}$$

The parameters determined from two different experiments using Eqs. 10 are compiled in Table I. From these experiments we obtain the average values $k_a^+ = 6.8 \times 10^6\ M^{-1}s^{-1}$ and $K_{0.5}^c = 35\ \mu M$. These values are close to previously published data obtained in the absence of caged ATP ($k_a^+ = 8$–$10 \times 10^6\ M^{-1}s^{-1}$ at 21°C and pH 7.5; Froehlich et al., 1976*a*, corrected with an activation energy of 68 kJ/mol; this corresponds to 1.2×10^7 at 24°C) or with a different technique ($K_{0.5}^c = 43\ \mu M$ at pH 7.2; Forbush, 1984). With $k_a^- = 94\ s^{-1}$ (see Results) and the k_a^+ determined in this

paper, we obtain an ATP binding constant of $K^a_{0.5}$ = 14 μM. This is somewhat larger as the value measured for pig kidney NaK-ATPase, $K^a_{0.5}$ = 2 μM (Nagel et al., 1987).

At high caged ATP concentrations ($c^0_c \gg K_{0.5}$), Eqs. B2 and 10 yield:

$$\tau_2^{-1} = \frac{\eta}{1-\eta} k_a^+ K^c_{0.5} \tag{11}$$

From Eq. 11 a straight line with slope $k_a^+ K^c_{0.5} \approx 240\ s^{-1}$ is expected in a plot of τ_2^{-1} vs. $\eta/(1-\eta)$. This is in agreement with the slope of 240 s^{-1} of the linear regression line shown in Fig. 7.

At $\eta = 0$ the regression line has a value of $\tau_2^{-1} = 20\ s^{-1}$ instead of starting at 0 as suggested by Eq. 11. This is possibly due to the fact that Eq. 11 is based on a linear kinetic model. However, the reaction cycle of the NaK-ATPase is closed and a significant turnover is measured even in the absence of K^+. Under these circumstances, the lowest possible value for the reciprocal relaxation time of the system is the rate constant of the rate-limiting step in the reaction cycle even though the rate constant of substrate binding approaches 0. This is analogous to a two-state model $A \rightleftharpoons B$. There the reciprocal relaxation time $\tau^{-1} = k^+ + k^-$ converges to k^- if k^+ goes to 0. The intercept of the regression line at 20 s^{-1} then has to be identified with the

TABLE I

Kinetic Parameters Determined from the Measurement of the Time Constants of the Electrical Signal at Varying Caged ATP Concentrations

η	$\overline{\tau_1^{-1}}$	$(\tau_2^{-1})_{max}$	$K_{0.5}$	k_a^+	$K^c_{0.5}$
0.23	302 s^{-1}	68 s^{-1}	46 μM	6.4 × 10^6 M^{-1} s^{-1}	36 μM*
0.18	265 s^{-1}	54 s^{-1}	38 μM	7.2 × 10^6 M^{-1} s^{-1}	34 μM

*Data from Fig. 6.

overall turnover of the system. Indeed, the rate-limiting step of the Na-ATPase has a comparable magnitude (6 s^{-1} in the absence of K^+, calculated from Hobbs, Albers, and Froehlich, 1985, with an activation energy of 80 kJ/mol).

An independent test of the assignment of τ_2^{-1} is the rapid mixing experiment in the presence of caged ATP (Fig. 8). An apparent rate constant for ATP binding of ~50 s^{-1} is obtained in these measurements. This is close to the value of 39 s^{-1} (see Table II, experiment 1), which characterizes the decay of the electrical signal in the bilayer control experiment.

According to the arguments given above, the decay of the electrical signal with time constant τ_2 has to be assigned to the binding of ATP and its exchange with bound caged ATP. A similar conclusion has been drawn for NaK-ATPase from pig kidney (Fendler et al., 1987). In particular, the ATP dependence of τ_2 rules out the possibility that the decaying phase of the signal has to be attributed to the electrogenic step as put forward by Apell et al. (1987).

It is instructive to compare the binding and dissociation rate constants for ATP and caged ATP. For caged ATP, $k_c^+ > 2.9 \times 10^7\ M^{-1}s^{-1}$ is calculated from the experimentally determined values $K^c_{0.5}$ = 35 μM and $k_c^- > 1{,}000\ s^{-1}$. The rate constants are larger than the corresponding rate constants for ATP, $k_a^+ = 6.8 \times 10^6$

$M^{-1}s^{-1}$ and $k_a^- = 94\ s^{-1}$. Both the larger binding rate constant and the much larger dissociation rate constant for caged ATP suggest that the steric requirements to accommodate the substrate molecule are less stringent than in the case of ATP. This may indicate a different binding geometry for caged ATP.

From a comparison of the simulated and the observed electrical signals, photolytic release of ATP from caged ATP in the binding site was excluded. There are at least two explanations for this effect: (*a*) After absorption of a photon the protective (2-nitro)phenylethyl group of caged ATP (Kaplan et al., 1978) cannot be split because the bound molecule does not have the degrees of freedom to break the essential bonds. (*b*) The caged ATP and the ATP binding sites are different but close enough to prevent binding of the other species if one binding site is occupied. Under such conditions, bound caged ATP can be photolytically transformed to ATP, but phosphorylation of the enzyme requires dissociation of the released ATP molecule

TABLE II

Fit Parameters to the Data Sets Shown in Fig. 2 Using Two Different Model Functions

Experiment 1 Model Function: Eq. 1			Experiment 2 Model function: Eq. 2			
τ_1^{-1}	190	±13	Fixed: $K_c^{0.5}$	35		μM*
τ_2^{-1}	39	±5	η_∞	0.20		
τ_3^{-1}	7.7	±0.2	k_p	450		s^{-1}‡
A_1	−0.7	±0.2	λ	407		s^{-1}§
A_2	0.5	±0.1	Variable: k_a^+	7.9×10^6	$\pm 0.5 \times 10^6$	$M^{-1}\ s^{-1}$
A_3	−0.05	±0.02	k_{12}	3,900	±2,000	s^{-1}
			k_s	1.6	±0.3	s^{-1}
			k_0	9.6	±0.2	s^{-1}

The average values and standard deviations of the parameters are calculated from the analysis of three (experiment 1) or four (experiment 2) different recordings obtained under the same conditions. In experiment 1, all listed parameters were adjusted during the fit, while in experiment 2 only the parameters termed variable were adjusted.

*From Table I, ‡from Fig. 8; §from Walker et al. (1988).

from the caged ATP binding side before it can rebind to the ATP binding site. At present, discrimination between the two mechanisms is not possible.

The Rising Phase of the Signal: The Electrogenic Step

It has been suggested previously (Fendler et al., 1987) that the electrical signals generated by the NaK-ATPase from pig kidney on lipid bilayers can be explained by a slow ATP-dependent reaction followed by a fast (100 s^{-1} at 22°C) electrogenic step. In this article, data obtained with NaK-ATPase from eel electric organ are analyzed. Qualitatively, the same behavior of the signals is found with somewhat larger rate constants than in the mammalian system. As shown in the previous section, the decay of the electrical signal described by τ_2 is due to ATP and caged ATP binding and exchange. Interpretation of the rising phase, however, is complicated by the fact that,

in addition to the time constants of the enzymatic cycle, electronic filtering and the release of ATP from its caged precursor are important in this time range.

Inspection of the signal in Fig. 2 shows a small but visible lag phase at the foot of the signal. This implies that the electrogenic step is preceded by at least two electroneutral processes. These are, however, not necessarily related to the partial reactions of the enzyme since, in addition to electroneutral enzymatic reactions, time constants of the measuring system also contribute to this part of the signal.

The lag phase in the case of experiment 1 in Fig. 2 is considerably longer than the lag in experiment 2 because of the use of the 500-Hz filter. To achieve better time resolution during the rising phase of the signal, experiment 2 in Fig. 2 and Table II was performed using the 1,000-Hz first-order filter. In this experiment, filtering ($\tau \approx 0.16$ ms) and one of the time constants of caged ATP binding and exchange ($\tau_+ \approx 0.12$ ms; Appendix B, Eq. B1) together account for a reciprocal relaxation time of only $\sim 3{,}000\ s^{-1}$ and will be neglected.

According to McCray, Herbette, Kihara, and Trentham (1980), ATP is released from caged ATP with a rate constant of $\sim 1{,}700\ s^{-1}$ at pH 6.2 and 24°C (corrected for the difference in temperature with an activation energy of 52 kJ/mol; Bárabas and Keszthelyi, 1984). Later, it was found that in the presence of 3 mM Mg^{2+} this rate constant decreases to $\sim 400\ s^{-1}$ at 24°C (Walker et al., 1988). Therefore, the rise of the signal ($\tau_2^{-1} \approx 190\ s^{-1}$; Table II) may be partially limited by ATP release. Since release and binding of ATP to the enzyme is not a first-order process, its contribution to the signal can be accounted for only approximately in terms of exponential components. An appropriate description of this part of the signal is given by the modified Albers-Post scheme defined in Eq. 2.

The kinetic model. The Albers-Post scheme (Fahn et al., 1966; Post et al., 1969) is the generally accepted kinetic model for the NaK-ATPase reaction cycle (Fig. 10). A basic feature of this model is the appearance of two enzyme conformations in the unphosphorylated (E_1 and E_2) and phosphorylated states (E_1P and E_2P). The different structural properties of these intermediates have been demonstrated with a variety of methods (Jørgensen and Andersen, 1988).

Conformational transitions are obvious candidates for electrogenic steps since in these transitions the ions are thought to be translocated across the dielectric barrier (Glynn, Karlish, and Yates, 1979). In addition, high resistance access channels leading to the ion binding sites have been discussed as a possible source of the electrogenicity of the pump (Läuger and Apell, 1988; Rakowski, Vasilets, LaTona, and Schwarz, 1991). Although these simple explanations are plausible, they are far from being conclusive. Since a protein is a charged macromolecule, any reaction during the catalytic cycle that displaces a portion of the molecule may give rise to an electrogenic reaction. This also includes the possibility for multiple electrogenic steps as observed, for example, in the light-driven proton pump, bacteriorhodopsin (Müller, Butt, Bamberg, Fendler, Hess, Siebert, and Engelhard, 1991).

Models for the transport activity of the NaK-ATPase with a single electrogenic step have been proposed by several authors (see, for example, Goldshlegger, Karlish, and Rephaeli, 1987; Bahinski, Nakao, and Gadsby, 1988). There is, however, experimental evidence that at least two electrogenic transitions are required in the presence of low concentrations of K^+ (Lafaire and Schwarz, 1986; Rakowski et al., 1991).

In the absence of convincing a priori knowlege about the number of nature of the electrogenic steps, we resorted to the simplest possible model, namely, a single electrogenic step in an otherwise electroneutral reaction cycle. Since the electrical experiments presented here were done in the absence of K^+, possible electrogenic steps in the K^+-dependent limb of the reaction cycle (Rakowski et al., 1991) can be ignored. The basis for the design of the reaction cycle was the condensed Albers-Post model (Eq. 2). As shown in Fig. 2, experiment 2, this simple model successfully reproduces the current measurements.

In the absence of K^+, dephosphorylation is slow ($\sim 6\ s^{-1}$ at 24°C, calculated from Hobbs et al., 1985, corrected for the difference in temperature based on an activation energy of 80 kJ/mol). It becomes fast if K^+ is added ($> 300\ s^{-1}$ at 21°C; Hobbs et al., 1985), while the rise and decay of the electrical signal remain approximately constant after addition of K^+ (Fendler et al., 1987). Therefore, the electrogenic event takes place before the decay of the E_2P intermediate and we have to consider the reaction sequence: $E_1 \rightarrow E_1ATP \rightarrow E_1P \rightarrow E_2P$.

In the presence of caged ATP, the apparent rate constant for ATP binding ($50\ s^{-1}$, Fig. 8) is smaller than in the absence of caged ATP ($120\ s^{-1}$, Fig. 8). A complete description of this process is possible using Eqs. 2–5 together with the parameters of Table I. This, together with the time dependence of the release of ATP from caged ATP, was included in the model (Eq. 2).

In the following, the electrical signal will be analyzed under the assumption that the $E_1P \rightarrow E_2P$ transition is the electrogenic step of the Na^+ part of the NaK-ATPase reaction cycle (Nakao and Gadsby, 1986; Apell et al., 1987; Fendler et al., 1987). However, a possible alternative interpretation, as, for example, an electroneutral $E_1P \rightarrow E_2P$ transition followed by a rapid electrogenic reaction in which Na^+ dissociation or rebinding occurs, is kinetically indistinguishable from this assumption. The term "$E_1P \rightarrow E_2P$ transition" will therefore be used in the sense as to include all kinetically indistinguishable alternatives.

Curve fitting. The parameters for the model (Eq. 2) are summarized in Table II, experiment 2. The release of caged ATP and the interaction of the enzyme with caged ATP and ATP is described by Eqs. 3 and 4 together with the parameters λ, η_∞ $K^c_{0.5}$, and k^+_a. The parameters k_p, k_{12}, and k_s refer to phosphorylation, the conformational transition, and the rate-limiting step, respectively. k_0 is the reciprocal system time constant.

Parameters termed "variable" and an additional scaling parameter were evaluated from the data by curve fitting (see Fig. 2). Those termed "fixed" were taken from other electrical or phosphorylation measurements described above or calculated according to Walker et al. (1988). For $K^c_{0.5}$, the fixed value from Table I was used since only the product $K^c_{0.5}k^+_a$ appears in Eq. 4 and an independent determination of $K^c_{0.5}$ and k^+_a is not possible. In addition, k_p and λ remained fixed because reliable estimates for these rate constants are available (see Table II). η_∞ is the fraction of ATP released from caged ATP after the photolytic reaction is completed. It corresponds to the η in all of the electrical experiments and was determined according to the procedure given in Materials and Methods.

The results of the fit are summarized in Table II, experiment 2. These values represent averages of fits to four different data sets obtained under the same

conditions. Good agreement between the model function and the data was obtained as shown in Fig. 2. This is also apparent from the reduced sum of squares for the fit given by $\chi^2_{red} = \Sigma_{i=1}^{n} (\langle I_i \rangle - I_i)^2/[\sigma^2(m - n)]$, where $\langle I_i \rangle$ and I_i are the calculated and the measured currents at time t_i, and n and m are the numbers of data points and parameters, respectively. The standard deviation of the data points, σ, was determined from the points sampled before the UV flash. The optimal value obtainable for χ^2_{red} is 1 (Bevington, 1969). For the four data sets analyzed, we obtained values ranging from 1.2 to 1.6.

As expected, k_a^+ and k_0 obtained by curve fitting are in good agreement with the values determined from the caged ATP dependence of the electrical signal. k_s corresponds to the rate constant of the rate-limiting step. Its value of 1.6 s^{-1} is not unreasonable in the absence of K^+. However, the data shown in Fig. 7 seem to require a rate-limiting step with a rate constant of $\sim$20 s^{-1}. The reason for this discrepancy is still unclear.

A remarkably large value for the rate constant for the $E_1P \rightarrow E_2P$ transition, k_{12} = 3,900 s^{-1}, was obtained. However, this value must be treated with caution because λ, k_p, and k_{12} are all of the same order of magnitude and all contribute to the rising phase of the signal. They are, therefore, highly correlated and cannot be determined independently from the electrical experiment (Müller and Plesser, 1991). This is also apparent in the larger error associated with the parameter k_{12} (Table II). Fortunately, the phosphorylation measurement shown in Fig. 8 provides a good estimate of k_p under the same conditions as the electrical measurements and λ is given by Walker et al. (1988).

To establish a more reliable estimate for k_{12}, one of the data sets was fitted with the model function given in Eq. 2 as described above, but with various fixed values of k_{12} and allowing k_a^+, k_s, k_0, and an additional scaling parameter to be adjusted. The values determined for k_{12} are highly dependent on k_p and λ. To take into account the uncertainty in k_p and λ, these parameters were allowed to vary between $\pm$10% of their nominal values. The reduced sum of squares at different values of k_{12} is shown in Fig. 11. The error limits of a parameter are given by its value at the point where χ^2_{red} has increased by 1 from its optimal value (Bevington, 1969). Therefore the optimal level $\chi^2_{red}(0)$ and the increased values $\chi^2_{red}(0)$ + 1 (labeled σ and corresponding to a confidence level of 68%) and $\chi^2_{red}(0)$ + 2 (labeled 2σ and corresponding to a confidence level of 95%) are included in the figure. From the results, it is clear that the fit can only provide a lower boundary for k_{12}. However, the steep rise in χ^2_{red} requires a minimum value for the rate constant for the $E_1P \rightarrow E_2P$ transition of $k_{12} \geq$ 1,000 s^{-1} at pH 6.2 and 24°C.

The $E_1P \rightarrow E_2P$ transition, Na^+ transport, and the electrogenic step. An underlying assumption in the Albers-Post model is that during the formation of E_2P Na^+ is translocated and released to the extracellular compartment. One way of testing this assumption is to use enzyme that has been modified so as to selectively block one of these reactions while leaving the others intact. An alternative method consists in directly comparing the kinetics of E_2P formation with that of Na^+ transport or release. However, in the literature there is no agreement about either the rate constant for the conversion of E_1P to E_2P or the rate constants for Na^+ translocation and release.

Rapid mixing techniques have been used in conjunction with acid quenching, fluorescence spectroscopy, and isotope filtration to obtain information about these reactions. From the time dependence of K^+ + EDTA-stimulated phosphoenzyme decay, Mårdh and Zetterqvist (1974) derived a rate constant of 77 s^{-1} for the rate of conversion of E_1P to E_2P at 21°C and pH 7.4. However, as discussed by Froehlich and Fendler (1991), the interpretation of these experiments is problematic and may not yield an appropriate value for the phosphoenzyme conformational transition. A more direct approach, which involves simultaneous measurement of transient state EP formation and P_i release in the presence of Na^+ and K^+, has been used to evaluate the kinetics of this transition in eel electric organ NaK-ATPase. By simulating the time course of these reactions according to the Albers-Post scheme, rate constants of 300 s^{-1}–1,000 s^{-1} at 21°C and pH 7.5 (Froehlich et al., 1983; Hobbs et al., 1985) and ~600 s^{-1} at 24°C and pH 6.2 (Froehlich and Fendler, 1991) have been obtained.

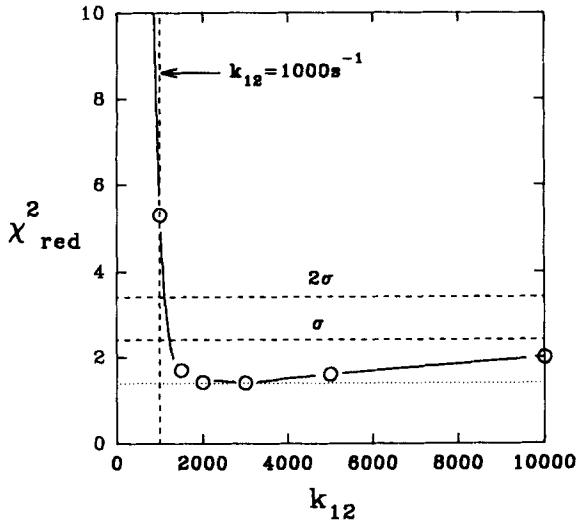

FIGURE 11. Reduced sum of squares χ^2_{red} of a fit to the data shown in Fig. 2, experiment 2 at different values of the parameter k_{12}. The dashed lines correspond to an increase of the optimal value of χ^2_{red} (*dotted line*) by 1 (σ) and 2 (2σ).

From the analysis of oligomycin inhibition of the NaK-ATPase Plesner (1991) also suggested a large rate constant (3,000 s^{-1} at 37°C and pH 7.4) for the E_1P to E_2P transition.

These rate constants are much larger than those obtained in stopped-flow fluorescence studies using potential-sensitive aminostyrylpyridinium dyes (Forbush and Klodos, 1991). They report values of 145 and 60 s^{-1} at 20°C and neutral pH for NaK-ATPase from eel electric organ and pig kidney, respectively. Other studies applied 5-iodoacetamidofluorescein-labeled NaK-ATPase from canine kidney (66 s^{-1} at 20°C and pH 7.0; Steinberg and Karlish, 1989) and *N*-[*p*-(2-benzimidazolyl)-phenyl]maleimide-modified NaK-ATPase from pig kidney (23 s^{-1} at 25°C and pH 7.4; Taniguchi, Suzuki, Kai, Matsuoka, Tomita, and Iida, 1984). Since the fluorescence change monitors the overall behavior of several steps including phosphoryla-

tion ($E_1 \rightarrow E_1P$) and the conformational transition ($E_1P \rightarrow E_2P$), these values have to be regarded as a lower boundary for the rate constant of the latter transition.

Rapid Na^+ extrusion from vesicles containing NaK-ATPase has been measured with a filtration technique using caged ATP and a UV flash to activate the enzyme (Forbush, 1984). The two reciprocal time constants describing the signal at 15°C were 14 and 6 s^{-1}, which are similar to the calculated values (18 and 5 s^{-1}) using the rate constant for release of ATP from caged ATP (Barabás and Keszthelyi, 1984; Walker et al., 1988) and the apparent rate constant of ATP binding in the presence of caged ATP under the conditions of Forbush (1984) (see Eq. 9 together with k_a^+ from Table II, corrected for the difference in temperature with an activation energy of 68 kJ/mol). More recent measurements of ATP-dependent transient fluorescence changes associated with EP formation using caged Mg^{2+} (Mg/DM-nitrophen; Kaplan and Ellis-Davies, 1988) have yielded a value of 45–50 s^{-1} (Forbush and Klodos, 1991), which is indistinguishable from the previously determined rate constant in the presence of caged ATP. These results suggest that the time dependence of the Na^+ transient is not entirely determined by the kinetics of ATP release or by the competition between ATP and caged ATP at the catalytic site.

Because of their probable association with charge translocation, electrical signals generated by the NaK-ATPase have been used to obtain information about the Na^+ translocation and release steps. From measurements of membrane potential-dependent steady-state currents in NaK-ATPase, it was concluded that at least one of the Na^+-dependent reactions of the enzymatic cycle is electrogenic (Nakao and Gadsby, 1989; Rakowski et al., 1989; Vasilets, Ohta, Noguchi, Kawamura, and Schwarz, 1993). Rate constants for a charge movement within the Na^+-dependent limb of the Albers-Post cycle have also been obtained from current transients measured in cardiac myocytes after a voltage step (Gadsby, Nakao, and Bahinski, 1991). At 20°C and pH 7.4, a rate constant of 40 s^{-1} was obtained, which is close to the values found in investigations utilizing the stopped-flow fluorescence and rapid filtration techniques.

Current transients generated by the purified NaK-ATPase on lipid bilayers as described in this work have previously been measured for enzyme prepared from pig (Fendler et al., 1985, 1987) and rabbit kidney (Borlinghaus et al., 1987). The rising phase of these signals with a relaxation time of $\tau = 10$ ms was attributed to an electrogenic step in the Na^+-dependent limb of the NaK-ATPase reaction cycle (Fendler et al., 1987). Subsequent analysis on the basis of the reduced photolysis rate constant of caged ATP in the presence of Mg^{2+} (Walker et al., 1988) now shows that the rise of the electrical signal in these measurements is partially limited by reactions other than the electrogenic step.

Using a chymotrypsin-modified enzyme, which is able to occlude Na^+ ions and catalyze phosphorylation and ADP/ATP exchange but is unable to undergo the $E_1P \rightarrow E_2P$ transition (Glynn, Hara, and Richards, 1984; Jørgensen and Petersen, 1985), Borlinghaus et al. (1987) demonstrated loss of the electrical signal after activation of the enzyme by photolytic release of ATP from caged ATP. These results clearly implicate a reaction downstream from phosphorylation, probably $E_1P \rightarrow E_2P$, in the electrogenic behavior.

Correlation of charge translocation measured by the bilayer method with the

conformational transition monitored by 5-iodoacetamidofluorescein labeling was attempted by Stürmer, Apell, Wuddel, and Läuger, (1989) using NaK-ATPase from rabbit kidney. In both the electrical and fluorescence measurements, the enzyme was activated by photolytic release of ATP from caged ATP. Under the conditions used in their experiments, the rate constants for ATP binding in the presence of caged ATP ($\sim 40\ s^{-1}$; see Eq. 9 corrected for the difference in temperature with an activation energy of 68 kJ/mol) and that for release of ATP from caged ATP ($\sim 25\ s^{-1}$; Barabás and Keszthelyi, 1984; Walker et al., 1988) were sufficiently small to suggest that those reactions might control the kinetic behavior of the electrical as well as the fluorescence signals. These considerations underscore the necessity of applying alternative methods with fewer complications or selecting conditions that minimize these effects in evaluating the kinetics of the NaK-ATPase partial reactions.

The electrical signal. From the observation of a lag phase in the electrical signal it was concluded that the electrogenic step is preceded by at least two electroneutral processes. The sequence of reactions that contribute to the electrical signal are: ATP release from caged ATP, ATP binding and exchange, phosphorylation, and the $E_1P \rightarrow E_2P$ transition. Therefore, both phosphorylation and the $E_1P \rightarrow E_2P$ transition are possible candidates for the electrogenic step. Since it is unlikely that the phosphorylation reaction is electrogenic (Borlinghaus et al., 1987), we have to conclude that the electrogenic reaction in the Na^+-dependent part of the NaK-ATPase reaction cycle involves the $E_1P \rightarrow E_2P$ transition. Therefore the model function given in Eq. 2 was based on an electrogenic $E_1P \rightarrow E_2P$ transition. Alternatively, a rapid ($k \gg 1{,}000\ s^{-1}$) electrogenic reaction (e.g., Na^+ release) after the $E_1P \rightarrow E_2P$ transition would also be compatible with our data.

As discussed above, the analysis of the electrical signal requires an $E_1P \rightarrow E_2P$ transition with a rate constant $\geq 1{,}000\ s^{-1}$. This rate constant is in agreement with values obtained from earlier quenched-flow studies involving measurements of phosphoenzyme formation and P_i release (Froehlich et al., 1983; Hobbs et al., 1985; Froehlich and Fendler, 1991). Also, the rate constant for enzyme from eel electric organ reported by Forbush and Klodos (1991) using aminostyrylpyridinium dyes is compatible with our measurements. If their fluorescence signal monitors the formation of E_2P, then phosphorylation ($\tau \approx 2$ ms; see Table II) and the time resolution of the stopped flow apparatus ($\tau \approx 3$ ms; Forbush and Klodos, 1991) also contribute to the measured time constant of $\tau \approx 7$ ms ($145\ s^{-1}$), leaving ~ 2 ms ($500\ s^{-1}$) to the $E_1P \rightarrow E_2P$ transition. Taking into account the difference in temperature of the two measurements we obtain a rate constant for the $E_1P \rightarrow E_2P$ transition of eel enzyme at 24°C of $650\ s^{-1}$. In view of the crude calculation, this result is remarkably close to the value of $\geq 1{,}000\ s^{-1}$ presented above.

Considerably different rate constants were determined in the filtration studies of Forbush (1984), in the fluorescence measurements of Steinberg and Karlish (1989), and in patch clamp studies (Gadsby et al., 1991). Possible reasons for these discrepancies are: (*a*) different pH (6.2 vs. 7.2–7.5), (*b*) different enzyme (eel electric organ vs. mammalian kidney), (*c*) different methods measure different reactions ($E_1P \rightarrow E_2P$ vs. Na^+ transport, release, or rebinding). This will be discussed below.

Electrical experiments conducted with NaK-ATPase from eel electric organ (data not shown) and pig kidney (Fendler et al., 1987) showed a decreased reciprocal

relaxation time of the rising phase of the signal (τ_1^{-1}) when increasing the pH from 6.2 to 7.2 or 7.7. This decline may be partly due to a decreased rate of release of ATP from caged ATP, which is only 34 s^{-1} at pH 7.3, 24°C, and 3 mM Mg^{2+} (Walker et al., 1988). Forbush and Klodos (1991) showed that the rate of the aminostyrylpyridinium dye signal increases with decreasing pH, but did not pursue these measurements below pH 7.2. If the rate constant doubles for each unit drop in pH as it does above pH 7.2, then the rate constant for the potential change monitored by the dye in the mammalian NaK-ATPase becomes 120 s^{-1}, which is a factor of 2–3 smaller than the reciprocal time constant for the rising phase of the electrical signal in the eel. This suggests that something in addition to pH is responsible for the slower kinetic behavior in the mammalian NaK-ATPase.

Part of the discrepancy mentioned above may be related to inherent differences in the properties of the enzymes prepared from different tissues. Indeed, 5- to 10-fold larger rate constants for some partial reactions of NaK-ATPase from aquatic tissue (shark salt gland; Esmann and Skou, 1988) as compared with enzyme from pig kidney have been reported. Moreover, the rise of the fluorescent signal using aminostyrylpyridinium dyes seems to be at least two times faster in enzyme from eel electric organ than in dog kidney enzyme (Forbush and Klodos, 1991). A similar factor of 2 comes from recent quenched-flow measurements with NaK-ATPase from pig kidney, demonstrating that the $E_1P \rightarrow E_2P$ transition is $\sim$400 s^{-1} at pH 6.2 and 24°C (unpublished data).

The general picture that emerges from these comparisons is that of a lack of agreement between results obtained with different methods that portend to measure the same kinetic process. Conceivably, the monitored reactions are different, requiring modification of the conventional Albers-Post scheme. A fast $E_1P \rightarrow E_2P$ transition and a slow Na^+ release (Forbush, 1987) or Na^+ translocation (Nakao and Gadsby, 1986) would require a more complex kinetic model, including, for example, a separate, relatively slow electrogenic Na^+ release step after the conformational transition. However, the close correlation of the rate constants determined from the phosphorylation experiments and the electrical measurements indicates that this step, if present in the reaction mechanism of the eel NaK-ATPase, must be very fast ($\gg$1,000 s^{-1}).

At present, no direct experimental evidence for a Na^+ deocclusion step in the eel enzyme is available as proposed for mammalian and amphibian enzyme (Läuger, 1991; Rakowski, 1991). It is, however, unlikely that the reaction mechanisms in different species differ in such a basic feature as the existence of a Na^+ deocclusion step. A more acceptable interpretation of our data is that this step is not observed in NaK-ATPase from electric eel because it is too rapid.

In summary, the electrical data obtained with the NaK-ATPase from eel electric organ are in quantitative agreement with the Albers-Post scheme and phosphorylation (Hobbs et al., 1985; Froehlich and Fendler, 1991) as well as fluorescence measurements (Forbush and Klodos, 1991) performed in the same tissue. The assignment of the current phases on the basis of the Albers-Post model suggests that the electrogenic step is the $E_1P \rightarrow E_2P$ transition, which is in agreement with assignments made for the electrogenic step of the NaK-ATPase in heart myocytes (Nakao and Gadsby, 1986), dog kidney (Apell et al., 1987), and pig kidney (Fendler

et al., 1987). In the eel tissue, this transition has a rate constant of at least 1,000 s^{-1} at pH 6.2 and 24°C. The disagreement with rate constants reported previously is probably due in part to a species difference.

Activation Energies

As shown in Fig. 4, linear Arrhenius plots were found for all time constants of the electrical signal. After the assignment of the different time constants of the signal as given above, only τ_1 and τ_2 correspond to transitions of the NaK-ATPase reaction cycle.

Esmann and Skou (1988) reported activation energies for NaK-ATPase and Na-ATPase activity from various tissues. For enzyme from shark rectal gland they determined activation energies of E_a = 64 kJ/mol and E_a = 90 kJ/mol for Na-ATPase and NaK-ATPase activity, respectively. These results are based on measurements of ATP hydrolysis and reflect the temperature dependence of the rate-limiting step. It is generally accepted that under the conditions used in their experiments, the rate-limiting steps for Na- and NaK-ATPase activity are the dephosphorylation ($E_2P \rightarrow E_2$) and the conformational transition ($E_2 \rightarrow E_1$), respectively.

In the electrical experiments, we determined activation energies of E_a = 101 kJ/mol and E_a = 68 kJ/mol for τ_1^{-1} and τ_2^{-1}, respectively. As discussed above, the rising phase of the signal described by τ_1^{-1} involves the $E_1P \rightarrow E_2P$ transition as well as phosphorylation and the release of ATP from caged ATP. Since the latter process has an activation energy of only 52 kJ/mol (Bárabas and Keszthelyi, 1984), the large temperature dependence of τ_1^{-1} indicates that a major contribution of this exponential component is not due to photolytic release of ATP. τ_2^{-1} corresponds to ATP/caged ATP binding/exchange. The activation energies obtained for the different time constants are all of a magnitude typical for a protein reaction.

The activation energies obtained by Esmann and Skou (1988) for enzyme from shark rectal gland are in good agreement with the data presented in this work. In particular, the activation energies for the reactions involving a substrate, like $E_1 \rightarrow E_1ATP$ (68 kJ/mol, eel) and $E_2P \rightarrow E_2$ (64 kJ/mol, shark) are very similar. Interpretation of the activation energy for the reaction characterized by τ_1 is complicated since, as discussed above, several processes contribute to this exponential component.

Conclusions

The electrical signal generated by the NaK-ATPase from the electric organ of *Electrophorus electricus* after an ATP concentration jump was analyzed and compared with the results of rapid mixing, quenched-flow experiments. It was shown that the slowest phase (τ_3) is related to the system time constant, which is characteristic of the compound membrane formed by the BLM and the adsorbed membrane fragments. The decaying (τ_2) phase of the electrical signal is assigned to the ATP/caged ATP binding and exchange reaction. Lag and rising phases correspond to the release of ATP from caged ATP, phosphorylation of the enzyme, and the electrogenic step, with the rate constants being of the same order of magnitude.

All data presented here for the NaK-ATPase from eel electric organ are consistent with a conventional Albers-Post model. Electroneutral ATP binding and phosphory-

lation are followed by a fast ($\tau^{-1} \geq 1{,}000\ s^{-1}$ at 24°C) electrogenic $E_1P \rightarrow E_2P$ transition. A rapid $E_1P \rightarrow E_2P$ transition is also in agreement with quenched-flow measurements performed with eel enzyme but seems to contradict the results of other studies with different methods. This may indicate that the Albers-Post model needs revisiting and/or that there is more than one electrogenic step involved in Na^+ transport.

APPENDIX A

Electrical Properties of the Compound Membrane

If first-order kinetics is assumed, a reaction scheme consisting of n intermediates yields a pump current given by:

$$I_p(t) = \sum_{i=1}^{n-1} a_i e^{-t/\tau_i} + b \tag{A1}$$

The time constants τ_i are the relaxation time constants of the reaction system and b is a stationary current.

The ion pump is coupled to the measuring device via the equivalent circuit shown in Fig. 1. The differential equations describing the circuit are:

$$\begin{aligned} \frac{dU_m}{dt} &= \frac{1}{C_m + C_p} I_p(t) - k_0 U_m \\ \frac{1}{C_m} I(t) &= \frac{dU_m}{dt} + k_m U_m \end{aligned} \tag{A2}$$

U_m is the voltage across the bilayer membrane. All other parameters of the equations are described in Results. The measured current $I(t)$ can be calculated from the pump current $I_p(t)$ by simple circuit analysis (Fahr et al., 1981; Borlinghaus et al., 1987):

$$I(t) = \frac{C_m}{C_m + C_p} \left(\sum_{i=1}^{n-1} a_i' e^{-t/\tau_i} + a_0 e^{-k_0 t} + b' \right) \tag{A3}$$

Comparison of Eqs. A1 and A3 shows that the relaxation times τ_i are not affected by the equivalent circuit. Only the amplitudes a_i and the stationary current b are changed. The amplitudes a_i' and the stationary current b' of the measured current $I(t)$ are:

$$\begin{aligned} a_i' &= a_i \frac{\tau_i^{-1} - k_m}{\tau_i^{-1} - k_0} \\ b' &= b \frac{k_m}{k_0} \end{aligned} \tag{A4}$$

In addition, the characteristic time constant of the equivalent circuit k_0^{-1} is introduced in the signal and has an amplitude a_0 of:

$$a_0 = b \frac{k_0 - k_m}{k_0} + \sum_{i=1}^{n-1} a_i \frac{k_m - k_0}{\tau_i^{-1} - k_0} \tag{A5}$$

Therefore, apart from a scaling factor $C_m/(C_m + C_p)$ the influence of the equivalent circuit

can be described by two parameters with a dimension of τ^{-1}:

$$k_0 = \frac{G_m + G_p}{C_m + C_p}$$
$$k_m = \frac{G_m}{C_m} \tag{A6}$$

which are determined by the conductances and capacitances G_m, G_p, C_m, and C_p of the membrane fragment/BLM compound membrane.

As evident from Eqs. A3–A5, the behavior of the current amplitudes a_i' is complicated when k_m or k_0 approaches τ_i^{-1}. The amplitude may disappear ($\tau_i^{-1} = k_m$), diverge ($\tau_i^{-1} = k_0$), or change sign ($\tau_i^{-1} < k_m, k_0 \rightarrow \tau_i^{-1} > k_m, k_0$).

APPENDIX B

Concentration Dependence of the ATP and Caged ATP Binding Reactions

The reaction sequence of Eq. 8 is characterized by two relaxation times τ_+ and τ_-. Their reciprocal values are given by Frost and Pearson (1953):

$$\tau_\pm^{-1} = \frac{B \pm \sqrt{B^2 - 4C}}{2}$$

with

$$B = [(1 - \eta)k_c^+ + \eta k_a^+]c_c^0 + k_c^-$$
$$C = \eta k_a^+ k_c^- c_c^0 \tag{B1}$$

k_c^- is the caged ATP dissociation rate constant and k_a^+ and k_c^+ are the second-order binding rate constants of the nucleotides. The relaxation times also depend on the concentration c_c^0 of caged ATP before the flash and the fraction η of released ATP.

The larger reciprocal relaxation time τ_+^{-1} starts at $\tau_+^{-1}(c_c^0 = 0) = k_c^-$ and increases rapidly with increasing caged ATP concentration. Since $k_c^{-1} \geq 1{,}000\ s^{-1}$, τ_+^{-1} at all caged ATP concentrations is much larger than the measured reciprocal time constants τ_1^{-1} and τ_2^{-1} and can therefore be neglected.

τ_-^{-1} is a saturating function of the caged ATP concentration, c_c^0. If the relation $B^2 \gg 4C$ holds, the square root can be approximated by the first two terms of a Taylor series:

$$\tau_-^{-1} \approx \frac{C}{B} = \eta k_a^+ K_{0.5} \frac{c_c^0}{c_c^0 + K_{0.5}} \tag{B2}$$

with

$$K_{0.5} = \frac{k_c^-}{(1 - \eta)k_c^+ + \eta k_a^+}$$

This is a hyperbolic saturation dependence where $K_{0.5}$ is the half-saturation concentration and $\eta k_a^+ K_{0.5}$ is the maximal value of the reciprocal relaxation time.

APPENDIX C

Differential Equations for Model 2

The differential equations describing the kinetic model of Eq. 2 are as follows:

$$\begin{aligned}
\frac{d[E_1]}{dt} &= k_s[E_2P] - k(t)[E_1] \\
\frac{d[E_1ATP]}{dt} &= k(t)[E_1] - k_p[E_1ATP] \\
\frac{d[E_1P]}{dt} &= k_p[E_1ATP] - k_{12}[E_1P] \\
\frac{d[E_2P]}{dt} &= k_{12}[E_1P] - k_s[E_2P]
\end{aligned} \tag{C1}$$

Initial conditions:

$$[E_1](0) = 1; \text{ all others are } 0.$$

We thank G. Schimmack and E. Grell for providing the caged ATP and E. Grabsch and E. Harbich for excellent technical assistance. Helpful discussions and critical suggestions for the improvement of the manuscript by E. Bamberg, H. J. Butt, K. Hartung, G. Nagel, K. Seiffert, and M. Stengelin are gratefully acknowledged. Major parts of this work were done while J. Froehlich was a guest scientist at the Max Planck Institute for Biophysics, Frankfurt, Germany.

This work was supported by the Deutsche Forschungsgemeinschaft (Sonderforschungsbereich 169).

Original version received 17 October 1991 and accepted version received 24 March 1993.

REFERENCES

Albers, R. W., G. J. Koval, and G. J. Siegel. 1968. Studies on the interaction of ouabain and other cardioactive steroids with the sodium-potassium-activated adenosine triphosphatase. *Molecular Pharmacology.* 4:324–336.

Apell, H.-J., R. Borlinghaus, and P. Läuger. 1987. Fast charge translocations associated with partial reactions of the Na,K-Pump. II. Microscopic analysis of transient currents. *Journal of Membrane Biology.* 97:179–191.

Bahinski, A., M. Nakao, and D. C. Gadsby. 1988. Potassium translocation by the Na^+/K^+ pump is voltage insensitive. *Proceedings of the National Academy of Sciences, USA.* 85:3412–3416.

Bamberg, E., H.-J. Apell, N. A. Dencher, W. Sperling, H. Stieve, and P. Läuger. 1979. Photocurrents generated by bacteriohodopsin on planar bilayer membranes. *Biophysics of Structure and Mechanism.* 5:277–292.

Barabás, K., and L. Keszthelyi. 1984. Temperature dependence of ATP release from "caged" ATP. *Acta Biochemica et Biophysica Academiae Scientiarum Hungaricae.* 19:305–309.

Benson, S. W. 1960. The Foundations of Chemical Kinetics. McGraw Hill Inc., New York. 39.

Berger, R. L., B. Balko, and H. F. Chapman. 1968. High resolution mixer for the study of the kinetics of rapid reactions in solution. *Review of Scientific Instruments.* 39:493–498.

Bevington, P. R. 1969. Data Reduction and Error Analysis for the Physical Sciences. McGraw Hill Inc., New York. 243.

Borlinghaus, R., H.-J. Apell, and P. Läuger. 1987. Fast charge translocations associated with partial reactions of the Na,K-Pump. I. Current and voltage transients after photochemical release of ATP. *Journal of Membrane Biology.* 97:161–178.

Clarke, R. J., H.-J. Apell, and P. Läuger. 1989. Pump current and Na/K coupling ratio of NaK-ATPase in reconstituted lipid vesicles. *Biochemica et Biophysica Acta.* 981:326–336.

De Weer, P., D. C. Gadsby, and R. F. Rakowski. 1988. Voltage dependence of the Na-K pump. *Annual Reviews in Physiology.* 50:225–241.

Esmann, M., and J. C. Skou. 1988. Temperature dependence of various catalytic activities of membrane-bound Na/K-ATPase from ox brain, ox kidney and shark rectal gland and of C12E8-solubilized shark Na/K-ATPase. *Biochemica et Biophysica Acta.* 944:344–350.

Fahn, S., G. J. Koval, and R. W. Albers. 1966. Sodium-potassium-activated adenosine tri-phosphatase of electrophorus electric organ. *Journal of Biological Chemistry.* 241:1882–1889.

Fahr, A., P. Läuger, and E. Bamberg. 1981. Photocurrent kinetics of purple-membrane sheets bound to planar bilayer membranes. *Journal of Membrane Biology.* 60:51–62.

Fendler, K., E. Grell, and E. Bamberg. 1987. Kinetics of pump currents generated by the Na^+, K^+-ATPase. *FEBS Letters.* 224:83–88.

Fendler, K., E. Grell, M. Haubs, and E. Bamberg. 1985. Pump currents generated by the purified Na^+K^+ATPase from kidney on black lipid membranes. *EMBO Journal.* 4:3079–3085.

Forbush, B., III. 1984. Na^+ movement in a single turnover of the Na pump. *Proceedings of the National Academy of Sciences, USA.* 85:5310–5314.

Forbush, B., III. 1987. Na^+,K^+, and Rb^+ movements in a single turnover of the Na/K pump. *Current Topics in Membrane and Transport.* 28:19–39.

Forbush, B., III, and I. Klodos. 1991. Rate-limiting steps in Na translocation by the Na/K pump. *In* The Sodium Pump: Structure, Mechanism, and Regulation. J. H. Kaplan and P. De Weer, editors. The Rockefeller University Press, New York. 211–225.

Froehlich, J. P., R. W. Albers, G. J. Koval, R. Goebel, and M. Berman. 1976*a*. Evidence for a new intermediate state in the mechanism of (Na + K)-adenosine triphosphatase. *Journal of Biological Chemistry.* 251:2186–2188.

Froehlich, J. P., and K. Fendler. 1991. The partial reactions of the Na- and Na^+K-activated adenosine triphosphatase. *In* The Sodium Pump: Structure, Mechanism, and Regulation. J. H. Kaplan and P. De Weer, editors. The Rockefeller University Press, New York. 227–247.

Froehlich, J. P., A. S. Hobbs, and R. W. Albers. 1983. Evidence for parallel pathways of phosphoenzyme formation in the mechanism of ATP hydrolysis by Electrophorus Na,K-ATPase. *Current Topics In Membranes and Transport.* 19:513–535.

Froehlich, J. P., J. V. Sullivan, and R. L. Berger. 1976*b*. A chemical quenching apparatus for studying rapid reactions. *Analytical Biochemistry.* 73:331–341.

Frost, A. A., and R. G. Pearson. 1953. Kinetics and Mechanism. John Wiley & Sons, Inc., New York. 1962.

Gadsby, D. C., and M. Nakao. 1989. Steady-state current–voltage relationship of the Na/K pump in guinea pig ventricular myocytes. *Journal of General Physiology.* 94:511–537.

Gadsby, D. C., M. Nakao, and A. Bahinski. 1991. Voltage-induced Na/K pump charge movements in dialyzed heart cells. *In* The Sodium Pump: Structure, Mechanism, and Regulation. J. H. Kaplan and P. De Weer, editors. The Rockefeller University Press, New York. 355–371.

Glynn, I. M., Y. Hara, and D. E. Richards. 1984. The occlusion of sodium ions within the mammalian sodium-potassium pump: it's role in sodium transport. *Journal of Physiology.* 351:531–547.

Glynn, I. M., S. J. D. Karlish, and D. W. Yates. 1979. The use of formycin nucleotides to investigate the mechanism of Na,K-ATPase. *In* Na,K-ATPase, Structure and Kinetics. J. C. Skou and J. G. Norby, editors. Academic Press Limited, London. 101–113.

Goldman, S. S., and R. W. Albers. 1973. Sodium-potassium activated adenosine triphosphatase. *Journal of Biological Chemistry.* 248:867–874.

Goldshlegger, R., S. J. D. Karlish, and A. Rephaeli. 1987. The effect of membrane potential on the mammalian sodium-potassium pump reconstituted into phospholipid vesicles. *Journal of Physiology.* 387:331–355.

Goldshleger, R., Y. Shahak, and S. J. D. Karlish. 1990. Electrogenic and electroneutral transport modes of renal Na/K ATPase reconstituted into proteoliposomes. *Journal of Membrane Biology.* 113:139–154.

Hobbs, A. S., R. W. Albers, and J. P. Froehlich. 1985. Quenched-flow determination of the E1P to E2P transition rate constant in electric organ Na,K-ATPase. In The Sodium Pump. I. Glynn and C. Ellory, editors. The Company of Biologists Limited, Cambridge, UK. 355–361.

Holz, M. 1990. Biophysikalische Signalanalyse mit kontinuierlichen Relaxationsspektren. Verlag für Wissenschaft und Bildung, Berlin.

Jørgensen, P. L., and J. P. Andersen. 1988. Structural basis for E1-E2 conformational transitions in Na,K-pump and Ca-pump proteins. *Journal of Membrane Biology.* 103:95–120.

Jørgensen, P. L., and J. Petersen. 1985. Chymotryptic cleavage of alfa-subunit in E1-forms of renal ($Na^+ + K^+$)-ATPase: effects on enzymatic properties, ligand binding and cation exchange. *Biochimica et Biophysica Acta.* 821:319–333.

Kanazawa, T., M. Saito, and Y. Tonomura. 1970. Formation and decomposition of a phosphorylated intermediate in the reaction of the Na-K-dependent ATPase. *Journal of Biochemistry.* 67:693–711.

Kaplan, J. H., and G. C. R. Ellis-Davies. 1988. Photolabile chelators for the rapid photorelease of divalent cations. *Proceedings of the National Academy of Sciences, USA.* 85:6571–6575.

Kaplan, J. H., B. Forbush III, and J. F. Hoffman. 1978. Rapid photolytic release of adenosine 5′-triphosphate from a protected analogue: utilization by the Na:K pump of human red blood cell ghosts. *Biochemistry.* 17:1929–1935.

Lafaire, A. V., and W. Schwarz. 1986. Voltage dependence of the rheogenic Na^+/K^+ ATPase in the membrane of oocytes of Xenpus laevis. *Journal of Membrane Biology.* 91:43–51.

Läuger, P., R. Benz, G. Stark, E. Bamberg, P. C. Jordan, A. Fahr, and W. Brock. 1981. Relaxation studies of ion transport systems in lipid bilayer membranes. *Quarterly Reviews of Biophysics.* 14:513–598.

Läuger, P., and H. J. Apell. 1988. Transient behaviour of the Na,K-pump: microscopic analysis of nonstationary ion-translocation. *Biochimica et Biophysica Acta.* 944:451–464.

Läuger, P. 1991. Kinetic basis of voltage dependence of the Na,K pump. *In* The Sodium Pump: Structure, Mechanism, and Regulation. J. H. Kaplan and P. De Weers, editors. The Rockefeller University Press, New York. 303–315.

Lowe, A. G., and J. W. Smart. 1977. The pre-steady-state hydrolysis of ATP by porcine brain (Na^+K)-dependent ATPase. *Biochemica et Biophysica Acta.* 481:695–705.

Mårdh, S. and Ö. Zetterqvist. 1974. Phosphorylation and dephosphorylation reactions of bovine brain (Na-K)-stimulated ATP phosphohydrolase studied by a rapid mixing technique. *Biochemica et Biophysica Acta.* 350:473–483.

McCray, J. A., L. Herbette, T. Kihara, and D. R. Trentham. 1980. A new approach to time-resolved studies of ATP-requiring biological systems: laserflash photolysis of caged ATP. *Proceedings of the National Academy of Sciences, USA.* 77:7237–7241.

Müller, K. H., H. J. Butt, E. Bamberg, K. Fendler, B. Hess, F. Siebert, and M. Engelhard. 1991. The reaction cycle of bacteriorhodopsin: an analysis using visible absorption, photocurrent and infrared techniques. *European Biophysics Journal.* 19:241–251.

Müller, K. H., and T. Plesser. 1991. Variance reduction by simultaneous multi-exponential analysis of data sets from different experiments. *European Biophysics Journal.* 19:231–240.

Nagel, G., K. Fendler, E. Grell, and E. Bamberg. 1987. Na^+ currents generated by the purified (Na^+ + K^+)-ATPase on planar lipid membranes. *Biochimica et Biophysica Acta.* 901:239–249.

Nakao, M., and D. C. Gadsby. 1986. Voltage dependence of Na translocation by the Na/K pump. *Nature.* 323:628–630.

Nakao, M., and D. C. Gadsby. 1989. [Na] and [K] dependence of the Na/K pump current–voltage relationship in guinea pig ventricular myocytes. *Journal of General Physiology.* 94:539–565.

Plesner, I. W. 1991. Order-of-magnitude estimation of rate constants for the interconversion of the phosphoenzymes of Na,K-ATPase, based on oligomycin inhibition experiments. *In* The Sodium Pump: Recent Developments. J. H. Kaplan and P. De Weer, editors. The Rockefeller University Press, New York. 345–349.

Post, R. L., S. Kume, T. Tobin, B. Orcutt, and A. K. Sen. 1969. Flexibility of an active center in sodium-plus-potassium adenosine triphosphatase. *Journal of General Physiology.* 54:306s–326s.

Provencher, S. W., and R. H. Vogel. 1983. Regularisation techniques for inverse problems in molecular biology. *In* Progress in Scientific Computing. P. Deuflhard and E. Hairer, editors. Birkhäuser Boston, Inc., Cambridge, MA. 304–319.

Rakowski, R. F. 1991. Stoichiometry and voltage dependence of the Na^+/K^+ pump in squid giant axons and *Xenopus* oocytes. *In* The Sodium Pump: Structure, Mechanism, and Regulation. J. H. Kaplan and P. De Weer, editors. The Rockefeller University Press, New York. 339–353.

Rakowski, R. F., D. C. Gadsby, and P. De Weer. 1989. Stoichiometry and voltage dependence of the sodium pump in volage-clamped, internally dialyzed squid giant axon. *Journal of General Physiology.* 93:903–941.

Rakowski, R. F., L. A. Vasilets, J. LaTona, and W. Schwarz. 1991. A negative slope in the current-voltage relationship of the Na/K-pump in Xenopus oocytes produced by reduction of external [K]. *Journal of Membrane Biology.* 121:177–187.

Schweigert, E. A. V. Lafaire, and W. Schwarz. 1988. Voltage dependence of the Na-K ATPase: measurements of ouabain-dependent membrane current and ouabain binding in oocytes of Xenopus laevis. *Pflügers Archiv.* 412:579–588.

Steinberg, M., and S. J. D. Karlish. 1989. Studies on conformational changes in Na,K-ATPase labeled with 5-iodoacetamidofluorescein. *Journal of Biological Chemistry.* 264:2726–2734.

Stürmer, W., H. J. Apell, I. Wuddel, and P. Läuger. 1989. Conformational transitions and charge translocation by the Na,K pump: comparison of optical and electrical transients elicited by ATP-concentration jumps. *Journal of Membrane Biology.* 110:67–86.

Taniguchi, K., K. Suzuki, D. Kai, I. Matsuoka, K. Tomita, and S. Iida. 1984. Conformational change of sodium- and potassium-dependent adenosine triphosphatase. *Journal of Biological Chemistry.* 259:154228–15233.

Vasilets, L. A., T. Ohta, S. Noguchi, M. Kawamura, and W. Schwarz. 1993. Voltage-dependent inhibition of the sodium pump by external sodium: species differences and possible role of the N-terminus of the α-subunit. *European Biophysics Journal.* 21:433–443.

Walker, J. W., G. P. Reid, J. A. McCray, and D. R. Trentham. 1988. Photolabile 1-(2-nitrophenyl)ethyl phosphatase esters of adenine nucleotide analogues: synthesis and mechanism of photolysis. *Journal of the American Chemical Society.* 110:7170–7177.